Cell. Mol. Life Sci. (2018) 75:301–322
https://doi.org/10.1007/s00018-017-2625-7

Cellular and Molecular Life Sciences

ORIGINAL ARTICLE

Dimerization leads to changes in APP (amyloid precursor protein) trafficking mediated by LRP1 and SorLA

Simone Eggert[1] · A. C. Gonzalez[1,7] · C. Thomas[1] · S. Schilling[1] · S. M. Schwarz[1,8] · C. Tischer[2] · V. Adam[1] · P. Strecker[1] · V. Schmidt[6] · T. E. Willnow[6] · G. Hermey[3] · C. U. Pietrzik[4] · E. H. Koo[5] · Stefan Kins[1]

Received: 24 February 2017 / Revised: 17 July 2017 / Accepted: 8 August 2017 / Published online: 10 August 2017

Abstract Proteolytic cleavage of the amyloid precursor protein (APP) by α-, β- and γ-secretases is a determining factor in Alzheimer's disease (AD). Imbalances in the activity of all three enzymes can result in alterations towards pathogenic Aβ production. Proteolysis of APP is strongly linked to its subcellular localization as the secretases involved are distributed in different cellular compartments. APP has been shown to dimerize in *cis*-orientation, affecting Aβ production. This might be explained by different substrate properties defined by the APP oligomerization state or alternatively by altered APP monomer/dimer localization. We investigated the latter hypothesis using two different APP dimerization systems in HeLa cells. Dimerization caused a decreased localization of APP to the Golgi and at the plasma membrane, whereas the levels in the ER and in endosomes were increased. Furthermore, we observed via live cell imaging and biochemical analyses that APP dimerization affects its interaction with LRP1 and SorLA, suggesting that APP dimerization modulates its interplay with sorting molecules and in turn its localization and processing. Thus, pharmacological approaches targeting APP oligomerization properties might open novel strategies for treatment of AD.

Keywords APP dimerization · APP processing · APP trafficking · APP transport · Alzheimer's disease

Introduction

The amyloid precursor protein (APP) is a key player in Alzheimer's disease (AD) since sequential cleavages by the

Simone Eggert and A. C. Gonzalez are first authors and contributed equally to this work.

Electronic supplementary material The online version of this article (doi:10.1007/s00018-017-2625-7) contains supplementary material, which is available to authorized users.

✉ Simone Eggert
s.eggert@biologie.uni-kl.de

✉ Stefan Kins
s.kins@biologie.uni-kl.de

[1] Department of Human Biology and Human Genetics, University of Kaiserslautern, Erwin-Schrödinger-Str. 13, 67663 Kaiserslautern, Germany

[2] EMBL, Heidelberg, Germany

[3] Institute for Molecular and Cellular Cognition, Center for Molecular University Medical Center Hamburg-Eppendorf, 20251 Hamburg, Germany

[4] Institute for Pathobiochemistry, Molecular Neurodegeneration, University Medical Center of the Johannes Gutenberg-University Mainz, 55099 Mainz, Germany

[5] Department of Neuroscience, University of California San Diego (UCSD), La Jolla, CA 92093-0662, USA

[6] Max Delbrueck Center for Molecular Medicine, Berlin, Germany

[7] Present Address: Institute for Biochemistry, Christian Albrechts University Kiel, 24118 Kiel, Germany

[8] Present Address: Institute for Medical Virology, University of Frankfurt, 60596 Frankfurt, Germany

enzymes β- and γ-secretases lead to the formation of the Aβ peptide, which accumulates in brains of AD patients [1]. APP is first cleaved by sheddases like α-secretase (ADAM10) [2] or β-secretase (BACE1) [3], leading to the release of the large ectodomain (sAPPα/sAPPβ) and the corresponding membrane-anchored C-terminal fragment (α-CTF/β-CTF) [4]. Those α- and β-CTFs can be further cleaved by γ-secretase [5] to release the soluble peptides p3 or Aβ, respectively, and the APP intracellular domain (AICD) [6, 7].

APP, a type I transmembrane protein [8], is co-translationally inserted into the ER and then transported through the secretory pathway via the *trans*-Golgi network (TGN) to the cell surface [9, 10]. APP gets internalized within minutes via clathrin-mediated endocytosis due to its "YENPTY" internalization motif presumably via the AP2 adaptor complex [11]. Following endocytosis, APP is delivered to early endosomes and can then be sorted in three different ways: (I) a fraction of APP recycles back to the cell surface [12, 13], (II) other APP molecules are transported retrogradely from endosomes back to the TGN in a retromer-mediated pathway [14], and (III), some APP molecules are trafficked to late endosomes which fuse to lysosomes where APP is degraded [15].

Processing by secretases occurs in different cellular compartments [9, 13]. APP is preferentially cleaved by α-secretase at the plasma membrane (PM) [16, 17]. In contrast, BACE1 cleavage of APP predominantly occurs in endosomes [3, 18]. After shedding by α- or β-secretase, γ-secretase cleavage takes place at the PM or in the endosomal/lysosomal system [19–21]. Thus, the subcellular localization of APP and the time spent in different cellular compartments directly affect its processing. Therefore, investigations on factors, which influence APP transport, are pivotal for the understanding of Aβ generation in AD.

Several studies have shown that APP can form lateral homo-dimers (*cis*-orientation), with the E1 domain of APP being the major dimerization interface [22, 23]. Further, APP *cis*-dimerization affects Aβ production [24–26], leading to the assumption that *cis*-dimerization might influence its transport and in turn its processing. It was shown that APP dimerization is initiated in the ER [27]. Using a BiFC (bimolecular fluorescence complementation) approach, it was reported that APP dimer formation occurs in different intracellular compartments, including ER, Golgi and/or endosomal structures [27, 28]. Furthermore, it has been demonstrated via a crosslinking approach that APP can form homo-dimers at the cell surface [22]. However, a detailed quantitative determination of APP localization in dependence of its dimerization state has not been performed yet.

Based on our previous studies [24], documenting an impact of APP dimerization on its processing, we provide here a detailed quantitative analysis of monomeric and dimeric APP subcellular localization using two independent inducible dimerization approaches. These data revealed that APP dimerization leads to an accumulation in the ER and in endosomes while it causes a decrease in the *cis*-Golgi. Further, we provide evidence that those changes might be caused by an altered interaction of APP dimers with LRP1 and SorLA.

Materials and methods

Plasmids

Generation of plasmids hAPP F1 pcDNA3.1+, hAPP F2 pcDNA3.1+, HA hAPP695 (L17C) pcDNA3.1+, HA hAPP695 (K28C) pcDNA3.1+ [24], HA hAPP695 pcDNA3.1+, myc hAPP695 pcDNA3.1+ [22], hSortilin WT pcDNA3.1− (zeo) [29], hSorLA WT pcDNA3.1+ (zeo) [29], hSorLA RFP pcDNA3.1+ (zeo) [30], hSorCS1cα Venus pcDNA3.1+ (zeo) [31], and myc hLRP1 CT (Domain IV) pLBCX [32] as well as myc hAPP695 (L17C) pcDNA3.1+ and HA hAPP695 (K28C) pcDNA3.1+ [24] has been described before. The plasmid pI-mRFP-KDEL pEGFP-C1 was a kind gift of Dr. Bruce Snapp [33]. For the cell surface marker IL2 td tomato, the cytoplasmic domain of the IL-2 receptor was replaced by td tomato [31].

N-terminally HA-tagged hAPP F1 in vector pC4 F1 (Clontech, Saint-Germain-en-Laye France) was generated as follows: HA APP695 pcDNA3.1+ was digested *Eco*RI–*Xho*I to obtain a 1037 bp fragment (fragment 1) including the N-terminal ORF of APP695. The C-terminal part of the APP ORF was generated via PCR with sense primer 5′ CGAGTT CCTACAACAGCAGCC 3′ starting before the APP internal *Xho*I site and antisense primer 5′ GCGGTGTCTAGAGTT CTGCATCTGCTC 3′ carrying an *Xba*I site. The PCR fragment was digested with *Xho*I and *Xba*I (fragment 2) and ligated together with fragment 1 in linearized Vector pC4F1 (Clontech, Saint-Germain-en-Laye France) (*Eco*RI/*Xba*I). The resulting plasmid encoding N-terminally HA-tagged APP F1 was validated by bi-directed sequencing.

Cell lines, transfections, and cell culture

N2a cells were maintained in culture media (MEM supplanted with 10% fetal bovine serum, 1% L-glutamine, 1% non-essential amino acids, 1% sodium pyruvate and 1% penicillin/streptomycin). N2a cells were not further differentiated with retinoic acid.

HeLa Kyoto cells were maintained in culture media (Dulbecco's modified Eagle's medium supplemented with 10% fetal bovine serum, 1% L-glutamine, and 1% penicillin/streptomycin).

For immunocytochemistry, HeLa cells were plated on glass coverslips in 24-well plates (Greiner, Frickenhausen, Germany) and transfected via the $CaPO_4$ method the following way: the culture media was replaced with fresh media 30 min to 1 h before transfection. 1 µg of DNA (2 × 0.5 µg for double transfection), 87 µl of Tris–HCl, pH 7.5, 12.4 µl of $CaCl_2$ were mixed and added under aeration to 100 µl 2× HBS (280 mM NaCl, 1.5 mM Na_2HPO_4, 50 mM HEPES, pH 7.12–7.13). The resulting solution was pipetted to one well of a 24-well plate and incubated at 37 °C, 5% CO_2 for 3 h. A glycerol shock was performed for 2 min and the cells were subsequently washed and maintained in culture media overnight.

The dimerizer, AP20187 (B/B) (Clontech, Saint-Germain-en-Laye France), was added 18 h post-transfection for 1 h. For western blot analysis, HeLa cells were transfected with jetPRIME (Polyplus, Illkirch, France) according to the manufacturer's instructions.

Primary cortical neurons were prepared using E14 embryos from C57BL/6J mice as described before [34]. The neurons were resuspended in DB1 medium [DMEM with 10% FBS, 0.79% D-glucose and 1× GlutaMAX (Thermo Fisher Scientific)] and subsequently plated on poly-L-lysine (Sigma-Aldrich)-coated fluorodishes (FD35-100, WPI Inc., Sarasota (USA)) at a density of $6 \times 10^5/cm^2$. After 6 h, DB1 media was changed and the neurons were cultivated in neurobasal medium supplemented with B27 and GlutaMAX (Thermo Fisher Scientific).

For live cell imaging analyses, primary cortical neurons were transiently transfected at DIV6 using calcium phosphate transfection [35].

Animals

C57BL/6J mice (E14) were used for generation of primary cortical neuron cultures. The sex of the species used is of either sex. Treatment of mice was in accordance with the German law for conducting animal experiments and followed the NIH guide for the care and use of laboratory animals. Animal housing, breeding, and euthanasia were approved by the German administration. All experimental protocols were carried out in accordance with the European Communities Council Directive of 24 November 1986 (86/609/EEC).

Antibodies

Primary mouse monoclonal antibodies included anti-HA antibody (000000011867431001, 3F10, Roche, Rotkreuz, Switzerland), anti-c-myc antibody (9E10) (Ab32, Abcam, Cambridge, UK), anti-GM130 antibody (610823, BD Biosciences, Heidelberg, Germany), anti-EEA1 (early endosomal antigen 1) antibody (610457, BD Biosciences, Heidelberg, Germany), Ab9, directed against the amino acids 1–16 of human Aβ [36], Syntaxin 6 (610635, BD Biosciences, Heidelberg, Germany), and calnexin (610523, BD Biosciences, Heidelberg, Germany). Further, the following rabbit polyclonal antibodies were used: anti-Lamp1 (ab24170, Abcam, Cambridge, UK), sAPPβ-specific antibody directed against the C-terminal end of wild-type human sAPPβ (JP18957, Immuno-Biological Laboratories, Inc., Minneapolis, MN), anti-c-myc (A-14, sc-769, Santa Cruz, Nunningen, Switzerland), anti-human Sortilin antibody (Prof. Peder Madsen, Aarhus, Denmark) [37], anti-GFP antibody (B2, sc-9996, Santa Cruz, Nunningen, Switzerland), and anti-SorLA antibody [29]. Further, the rabbit monoclonal antibody Y188 with the epitope in the APP C terminus was used to detect endogenous APP (1565-1, Epitomics, Burlingame, United States). Specificity of this antibody has been shown [34, 38].

Immunocytochemistry

HeLa cells were plated at a density of 35.000 cells per 24-well plate (Greiner, Frickenhausen, Germany), on 14-mm coverslips (Marienfeld, Lauda-Königshofen Germany) and transfected via $CaPO_4$ (see above). For intracellular staining, the cells were fixed after 18–20 h for 10 min at 37 °C in 4% PFA (Sigma, Deisenhofen, Germany) with 4% sucrose and permeabilized for 10 min with 0.1% NP40. After incubation of primary antibodies at 4 °C overnight and secondary antibodies for 1 h at room temperature (RT) (Alexa Flour 488, Alexa Flour 594 (Invitrogen, Karlsruhe, Germany), cells were embedded in Mowiol (Sigma-Aldrich, Steinheim, Germany) and subjected for imaging with the software Axiovision 4.8 at the microscope Axio Observer Z.1 (Zeiss, Jena, Germany).

For cell surface stainings, HeLa cells were transfected with different N-terminally c-myc- or HA-tagged APP encoding expression plasmids. 18–20 h post-transfection, the cells were incubated for 1 h with 100 nM dimerizer, AP20187 (B/B) (Clontech, Saint-Germain-en-Laye France) or EtOH (control). To stop endocytosis, the 24-well plate was cooled down on iced water and incubated with c-myc or HA primary antibodies for 1 h at 4 °C. After a washing step, the cells were fixed with 4% PFA for 30 min. The cells were washed again and incubated with secondary antibodies (Alexa Flour 488 (Invitrogen, Karlsruhe, Germany) for 1 h at RT. Before the cells were permeabilized in 0.1% NP40 in PBS for 10 min at RT, residual secondary antibody was removed carefully. A blocking step followed in 5% goat serum/PBS. For detection of intracellular APP, the cells were incubated with the same primary antibody as for cell surface APP for 1 h at 4 °C, but subsequently with a different secondary antibody (Alexa-594, Invitrogen, Karlsruhe, Germany) for 1 h at RT. After further washing steps, the

coverslips were placed upside down in 30 µl pre-warmed Mowiol (Sigma-Aldrich, Steinheim, Germany) and subjected to microscopic analysis.

Quantification of APP within different intracellular cell organelles

For quantification of co-localization of APP within different organelles, specifically designed pipelines for CellProfiler 2.1.0 [39] were used. Co-localization with the ER marker (KDEL) was based on Pearson correlation, with values ranging from −1 (perfect exclusion) to 1 (perfect co-localization). An object-based analysis of APP localization was used for the Golgi apparatus, early endosomes and lysosomes. One medial layer of the images was chosen for the analysis. Then, a mask of the cell (to define the area of measurement) and a background rectangle (which does not include signals from any other cell) was drawn. Based on the background corrected measurements of APP signal in the respective organelle and in the whole cell, the fraction of APP localizing to the organelle was computed. Output images showing the cell and object segmentations were produced for visual control of the image analysis.

Quantification of total versus cell surface APP

Direct comparison of immunostainings of cell surface APP and total APP signal was used for quantification. For quantification of cell surface APP, again a specifically designed pipeline for the CellProfiler 2.1.0 software [39] was used. Here, *z*-stack image projections for both, cell surface APP and intracellular APP, were analyzed. The distance between single optical sections in *z*-direction were set to 0.2 µm and subsequently sum-projections of our *z*-stack images were performed. Due to the weaker signal of cell surface APP immunoreactivity respective to the total signal, the images of cell surface APP were taken using a fixed ratio of the exposure times for cell surface and total APP immunoreactivity. Therefore, both channels had a comparable intensity signal for surface and total APP, independent of individual APP expression levels. Notably, for analysis only cells with moderate comparable expression levels of APP were chosen. With this method, background noise for the relatively weaker cell surface staining was avoided. Further, microscope equipment and settings were: Zeiss microscope Axio Observer. Z1, HXP120C, Software Axiovision Release 4.8, 63x immersion oil objective, filter settings: GFP (green) = set38 (BP 470/40, FT 495, BP 525/50); propidium-iodide (red): set00 (BP 530-585, FT 600, LP 615).

Cell surface intensity and intracellular intensity were measured for each cell. As explained before, we computed a ratio of intracellular to cell surface signal. Those ratios were normalized to the ratio measured in the control samples. An output image as well as the necessary intensity values for quantification was produced.

Antibody uptake assay (endocytosis assay)

N2a cells expressing N-terminally c-myc-tagged APP were placed on iced water to stop endocytosis and incubated with primary anti-c-myc antibody for 30 min. After removal of the antibody, endocytosis was allowed by incubating each plate for 5, 10 or 15 min at 37 °C. Afterwards the cells were fixed with 4% PFA (Sigma, Deisenhofen, Germany). Immunocytochemical stainings were performed, as described for cell surface APP and internalized APP. Z-stack image projections for both fluorescent signals were analyzed. Cell surface intensity and intracellular intensity were measured for each cell. The ratio of endocytosed fluorescence signal to cell surface APP (internalized versus cell surface protein) was calculated and those ratios were normalized to the ratio measured in the control samples at 0 min.

Live cell imaging

Live cell imaging analysis was performed as described previously [10, 31]. For analysis of dimerized APP, neurons were treated 10 min before starting the recording with EtOH (negative control) or 100 nM dimerizer (AP20187 (B/B), Clontech, Saint-Germain-en-Laye France). Live cell imaging was carried out with the feature "Fast Image Acquisition" (software Axiovision 4.8) using fast changing LEDs [microscope Axio Observer Z.1 (Zeiss, Jena, Germany)]. The recordings were performed over a time span of 30 s with intervals of 200 ms and exposure times of 10–150 ms. Blinded live cell recordings were analyzed with ImageJ (Wayne Rasband, National Institute of Health, USA) using the multiple kymograph plugin. The resulting vesicle traces were marked with the "Multiple Point Tool" at both ends. The tracing was performed for anterograde and retrograde vesicles independently. The slopes of traces with a minimal length of 0.113 µM were taken for determination of vesicle velocity.

Co-immunoprecipitation

Co-immunoprecipitations were performed, as described before [40]. Briefly, HeLa cells co-expressing APP695 F1 (includes a C-terminal HA tag) and one member of the Vps10p domain receptor family (hSorCS1cα Venus, hSortilin WT, hSorLA RFP) or myc hLRP1 CT were harvested and lysed in 50 mM Tris/HCl, pH 7.5, 150 mM NaCl, 5 mM EDTA, 1% NP40, 1:25 protease inhibitor (Complete (with EDTA), Roche, Rotkreuz, Switzerland) 18 h post-transfection. Equal volumes of cell lysates containing ~1000 µg protein were precleared with 10 µl of Protein A Sepharose (GE

Healthcare, Freiburg, Germany) for 1 h at 4 °C. Afterwards, the supernatant was incubated at 4 °C overnight with 20 µl of anti-HA antibody-coated beads (Roche, Rotkreuz, Switzerland) at RT. After several washing steps with lysis buffer and 10 mM Tris/HCl, pH 7.5, the beads were resuspended in SDS sample buffer (0.125 M Tris/HCl, pH 6.8; 20% glycerol; 4% SDS; 0.01% bromphenol blue; 100 mM DTT) and incubated for 5 min at 95 °C. The samples were loaded on an 8% Tris/glycine gel and subjected to western blot analysis using different primary antibodies.

Subcellular fractionation

An iodixanol [(Optiprep), Sigma, Deisenhofen, Germany] gradient fractionation of cell lysates (HeLa cells) was performed. For analysis of heterologously expressed N-terminally HA-tagged APP WT, K28C and L17C, two transiently transfected (JetPrime) 10-cm dishes were used. To investigate endogenous APP monomers and dimers, five non-transfected 10 cm dishes of HeLa cells were pooled. The cells were washed one time with ice-cold 1× PBS and scraped for collection in 1.8 ml of PBS. After centrifugation for 10 min at 5000 rpm at 4 °C in a tabletop microcentrifuge the cell pellets were resuspended and pooled in 1 ml of homogenization buffer (1× Hom buffer pH 7.4), 300 mM sucrose, 10 mM HEPES, pH 7.4, 5 mM EDTA, pH 8.0, and protease inhibitor "Complete" (PI) (Roche). The cells were disrupted by 10 passages through a 25 G needle and 5 passages through a 27 G needle. The homogenate was centrifuged for 5 min at 1200 rpm (4 °C) and the post-nuclear supernatant (PNS) was collected. A 5–40% iodixanol gradient was prepared using 3× Hom buffer, pH 7.4. 0, 5, 10, 15, 20, 30, 40% iodixanol samples were layered underneath in a thin-wall ultracentrifugation tube and a continuous gradient was obtained using a gradient mixer (Biocomp, Gradient Master, Nycomed Pharma). The PNS was layered on top of the gradient and the samples were centrifuged for 2 h at 150,000×*g* in an SW41Ti rotor with deceleration. 15 fractions were taken from each gradient and equal volumes of each fraction were analyzed on an 8% Tris/glycine gel.

Cell surface biotinylation

5×10^5 HEK293T cells were seeded on a six-well plate. The following day the cells were transiently transfected with JetPrime with HA APP WT pcDNA3.1+, HA K28C pcDNA3.1+ or HA L17C pcDNA3.1+. Non-transfected cells served as a negative control. In a different set of experiment, myc-APP F1 pcDNA3.1+ was transiently transfected in HEK293 cells. Non-transfected cells served again as a negative control. The next day, HEK293 cells heterologously expressing APP F1 were incubated with 200 nM, 500 nM AP20187/dimerizer or EtOH as vehicle control for 1 h before analysis. The cells were rinsed twice with ice-cold 1× PBS and incubated for 30 min at 4 °C with 1 ml of EZ-Link Sulfo-NHS-LC-Biotin (Pierce) (2 mg/ml) in ice-cold PBS to biotinylate surface proteins. To quench unconjugated biotin, the cells were washed three times with 1× PBS supplemented with 100 mM glycine. Cells were lysed in 1× RIPA buffer [20 mM Tris/HCl, pH 8.0; 150 mM NaCl; 1% NP-40 (w/v); 0.5% deoxycholate; 5 mM EDTA, pH 8.0; 0.1% SDS, 1:25 protease inhibitor (Complete (with EDTA), Roche)] and 20 µg of lysate was used for the direct load. Equal protein amounts were incubated with NeutrAvidin Agarose Resin (Pierce) overnight at 4 °C. The following day the beads were washed with RIPA buffer and boiled at 95 °C for 5 min in 2× sample buffer with DTT to recover the biotinylated proteins. Direct load and surface proteins were separated on an 8% Tris/glycine gel [34].

Western blot

Western blot was performed using standard methods as described [24]. Briefly, cells were lysed for 15 min at 4 °C in lysis buffer (50 mM Tris/HCl, pH 7.5, 150 mM NaCl, 5 mM EDTA, and 1% Nonidet P40) supplemented with protease inhibitors (Complete™ protease inhibitor mixture, Roche Applied Science). The supernatants were collected and the protein concentration was determined with a BCA assay (Sigma). Equal amounts of protein samples were separated on 8% Tris/glycine SDS-PAGE and then transferred to nitrocellulose membranes. Subsequently the membranes were incubated with primary antibodies and HRP-coupled secondary antibodies. Chemiluminescence was measured using an imager and the software Fusion.

Results

Extending our previous study on APP dimerization affecting APP processing [24], we tested if dimerization of APP might alter its subcellular localization. As in our previous study, we used again two different assay systems: (1) mutant APP carrying an additional cysteine residue forming constitutive dimers and (2) APP mutants fused to FK506-binding protein (FKBP), allowing to induce dimerization by addition of a rapamycin analogue (Fig. 1).

Induced controlled dimerization with the FKBP system

The inducible dimerization system is based on the 12-kDa human FKBP 506-binding protein (FKBP12, also called FKBP) and a small ligand. FKBP is a monomeric and highly abundant cytosolic protein which serves as a primary receptor for the immunosuppressive ligands FK506 and rapamycin [41]. The regulated dimerization of two FKBP molecules

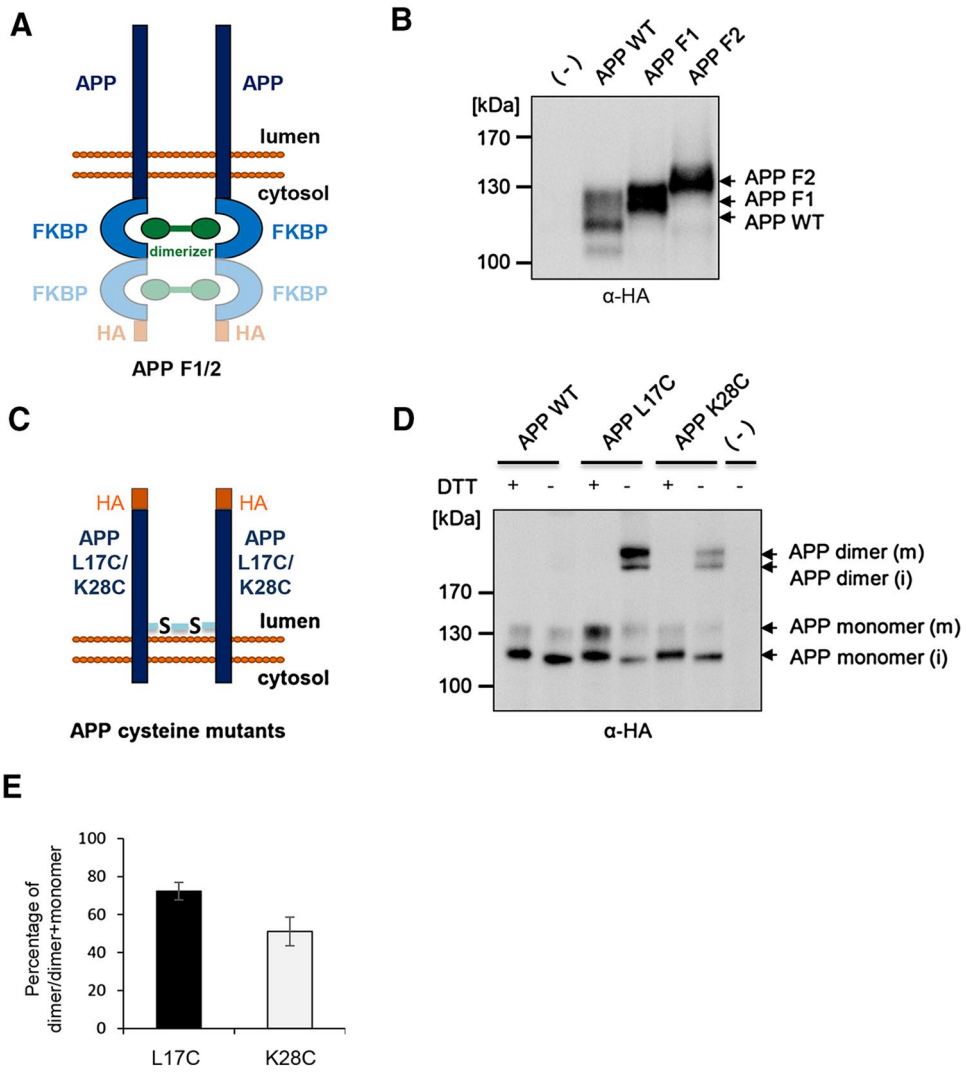

Fig. 1 FKBP-based and cysteine-induced dimerization. **a** Schematic representation of APP F1 and APP F2 dimerization systems. APP was fused to either one FKBP (APP F1) or two FKBP (APP F2) domains followed by an HA-tag. The AP20187 ligand (dimerizer) binds two FKBP molecules thereby inducing dimerization of APP (modified from [24]). **b** APP WT, APP F1, and APP F2 (all C-terminally HA tagged) were heterologously expressed in HeLa cells and equal protein amounts of cell lysates (with DTT) were analyzed via western blot detection with α-HA antibody. **c** Schematic representation of the APP cysteine mutants (L17C and K28C), engineered to form constitutive APP dimers via disulfide bonds. **d** HeLa cells were transiently transfected with N-terminally HA-tagged APP L17C/K28C constructs and compared with N-terminally HA-tagged APP695 WT (APP WT). Non-transfected (NT) cells were used as a negative control. Equal amounts of protein were denatured in sample buffer with and without DTT and analyzed via western blot detection with α-HA (3F10) antibody. The immature (i) and mature (m) forms of APP monomers and APP dimers are indicated. **e** Quantification of densitometric measurements of western blots of APP dimers compared to APP total for mutants HA L17C and HA K28C ± SEM (n = 3)

can be induced by addition of a small membrane permeable rapamycin analogue, AP20187 [41]. AP20187 binds simultaneously to two FKBP molecules thereby inducing dimerization. To eliminate the ability of rapamycin to bind endogenous FKBP, the affinity and specificity of this molecule was improved by a single amino acid substitution within the FKBP tag. The rapamycin analogue AP20187 can bind with subnanomolar, 1000-fold higher affinity to the mutated FKBP tag compared to endogenous wild-type FKBP [41].

In the present study a chimeric APP construct was used, encoding human APP695, which was C-terminally fused to the FKBP (F1) domain (APP F1) or two FKBP (F2) domains (APP F2) followed by an HA epitope tag (Fig. 1a, b) [24]. Comparable heterologous expression of both APP F1 and APP F2 fusion proteins was evaluated by western blot analysis. Signals for monomeric APP F1 and APP F2 were observed at ~135 and ~150 kDa, respectively. Due to the additional one or two FKBP tags the

apparent molecular weight is slightly increased compared to APP WT (~120 kDa) (Fig. 1b).

It has already been shown via western blot after blue native PAGE under semi-denaturing conditions in samples without SDS that dimer formation of APP F1 and APP F2 indeed occurs by non-covalent interactions [24]. APP F1 is dimerized up to 70% and APP F2 up to 90% when 100 nM dimerizer AP20187 was added, while in control samples under non-induced conditions, APP is dimerized only to about 5% [24].

Constitutive dimerization via cysteine mutants

For the second dimerization system, two different constitutive dimerization constructs were engineered to form stable dimers by introducing cysteine substitutions into the juxtamembrane region of APP695 at positions L17 and K28, termed APP L17C and APP K28C, respectively [24, 25, 42]. An HA-tag was introduced at the N terminus of both mutants (Fig. 1c). The cysteine mutants were evaluated after heterologous expression in HeLa cells by western blot analysis (Fig. 1d). N-terminally HA-tagged APP695 WT (APP WT) was compared to APP L17C and APP K28C in samples prepared with and without DTT. Both, immature (*N*′-glycosylated) and mature (*N*′ and *O*′-glycosylated) forms of monomeric APP were detected for all constructs (Fig. 1d). The mutants L17C and K28C show two clear signals at the predicted apparent molecular mass of APP dimers (~240 kDa), representing presumably also immature and mature dimeric forms of APP, with the strongest effect for L17C. The presence of immature APP dimers is consistent with the assumed APP dimer formation in the ER. Also for the APP WT control, a very weak signal of dimer formation was observed. As expected, no intermolecular disulfide bonds were formed under reducing conditions (+DTT) (Fig. 1d). This shows that both mutants (APP L17C and APP K28C) exist predominantly in the form of covalently bound stable APP dimers (72.35 ± 4.53 and 51.1 ± 7.59%, respectively) (Fig. 1e).

Together with our previous published data [24], these results show that heterologously expressed APP is only dimerized to about 5% in HeLa cells while the APP cysteine mutants form constitutive dimers up to 51.1% (K28C) and 72.35% (L17C). The addition of dimerizer to APP F1 or APP F2 caused dimer formation up to 70% (APP F1) or 90% (APP F2) as well. Thus, both systems are suitable to analyze the influence of dimeric APP compared to monomeric APP in regard to its transport and localization in HeLa cells.

Comparative analysis of APP monomers/dimers by subcellular fractionation and flourescence microscopy

We sought to determine the subcellular localization of APP monomers and dimers. For this purpose, we decided to examine their distribution by subcellular fractionation (Fig. 2) and via fluorescence microscopy (Figs. 3, 4, 5). For subcellular fractionation experiments, we used non-transfected HeLa cells expressing endogenous APP or cells expressing recombinant wild-type APP, APP L17C and APP K28C. The different HeLa cell extracts were kept in reducing (Fig. 2a) or non-reducing (Fig. 2b) conditions, allowing detection of monomeric APP and stable cysteine-bond APP dimers. Homogenates were separated on a 0–40% iodixanol OptiPrep gradient to isolate fractions enriched in different subcellular membranes. Calnexin was used as a marker for the ER, GM130 as *cis*-Golgi marker, Syntaxin 6 as TGN marker and EEA1 as a marker for early endosomes. Western blot analyses of the gradient-derived fractions are presented in Fig. 2. Cysteine-bond dimers from recombinant wild-type APP were detected similar to its monomeric form in most of the different subcellular fractions, whereby only small amounts were present in the endosomal fractions. Similarly, endogenous monomeric APP was visualized mostly in the Golgi and ER containing fractions. Increased levels of certain mature and immature APP species were also evident, likely reflecting post-translationally modified APP751 or APP770. Surprisingly, low levels of endogenous DTT-sensitive cysteine-bond APP dimers were only detected in the endosomal fraction. This suggests that stable APP dimers accumulate in endosomes. In line with this, we found that cysteine-bond dimers of APP L17C and APP K28C were also enriched in endosomal fractions (Fig. 2).

To validate our results from the subcellular fractionation experiments and to allow a better determination of the subcellular localization of APP dimers, we performed immunocytochemical studies of HA-tagged wild-type APP, APP L17C, and APP K28C. The immunofluorescence images of wild-type APP show a characteristic distribution with a clear accumulation in the perinuclear region (presumably Golgi apparatus) and a vesicular pattern throughout the cell periphery (Fig. 3). The subcellular distribution of APP L17C and APP K28C, exhibiting increased levels of stable APP dimers, showed a slightly altered subcellular localization compared to APP wild type (Fig. 3; Fig. S1). The accumulation in the perinuclear region appeared diminished and instead a wider distribution of punctate staining all over the cytoplasm was observed. Using different markers for the endoplasmic reticulum (ER) (KDEL-mRFP),

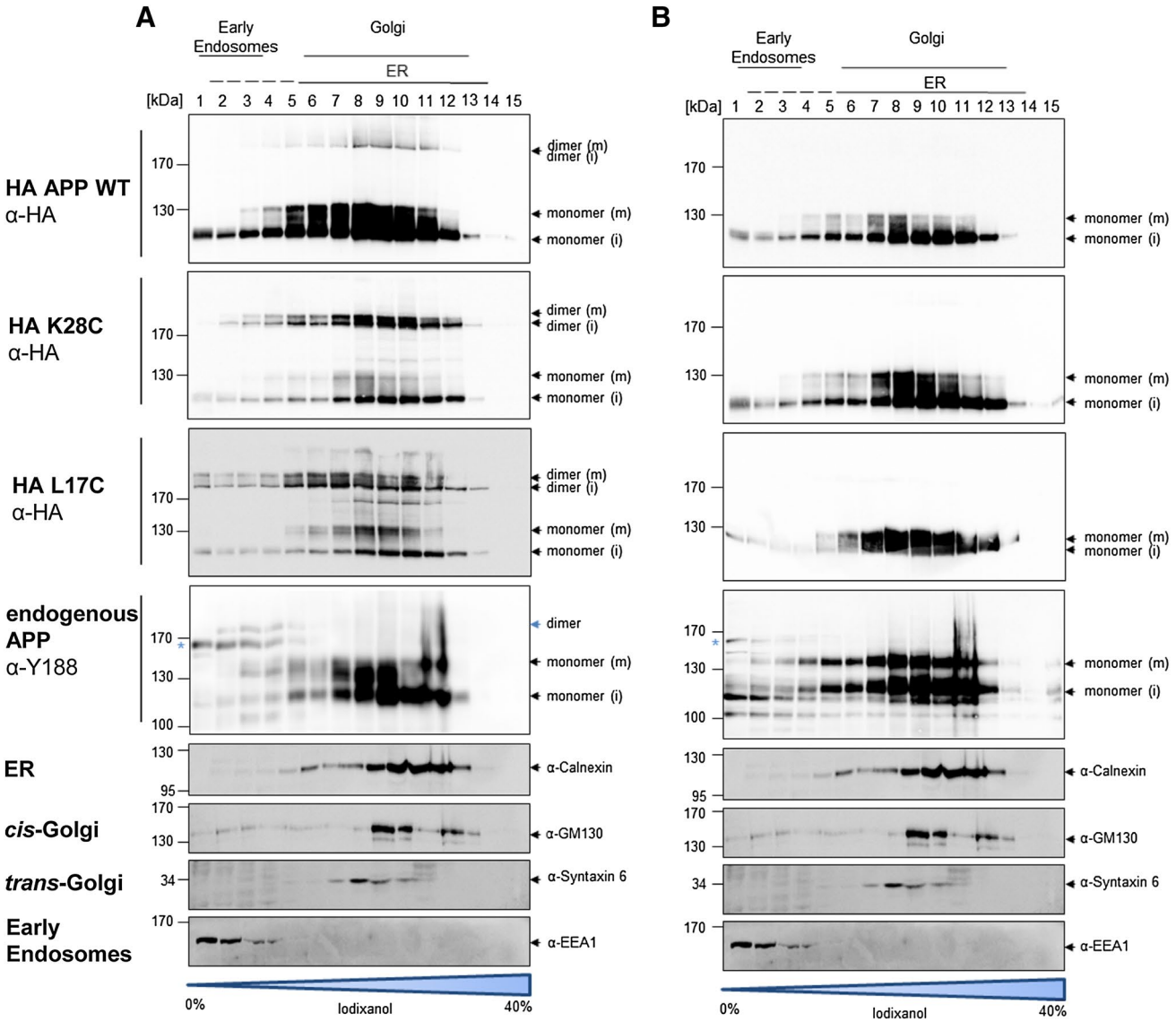

Fig. 2 Subcellular fractionation of cysteine-bond dimers: HeLa cells expressing N-terminally HA-tagged APP WT and APP K28C and L17C or non-transfected cells were fractionated via a continuous 0–40% iodixanol (Optiprep) gradient. Equal volumes of the samples were analyzed in samples without DTT (**a**) or samples with DTT (**b**) to obtain monomeric APP only. Western blot detection of heterologously expressed HA APP, HA APP K28C, and HA APP L17C followed with α-HA antibody 3F10 and endogenous APP with the APP-specific antibody Y188. Anti-calnexin antibody was used to detect the ER, α-GM130 antibody to detect the *cis*-Golgi apparatus, α-synatxin 6 the *trans*-Golgi apparatus and α-EEA1 to reveal early endosomes. The *blue star* indicates a monomeric, possibly post-translationally modified form of APP

cis-Golgi (anti-GM130 antibody), early endosomes (anti-early endosomal antigen 1 (EEA1) antibody), we analyzed the localization of APP wild type, APP L17C, and APP K28C within different intracellular compartments. For quantification, a Pearson correlation coefficient was used to measure the linear correlation between the intensity of the APP (monomer or dimer) signal and its signal intensity in the ER (Fig. S1). The quantification shows an increase for stable cysteine-bond APP dimers only in endosomes (Fig. 3).

Further, we analyzed the alteration in subcellular distribution after induced dimer formation of APP F1 and APP F2 forming non-covalent bound APP dimers (Fig. 4). For monomeric APP F1 and APP F2 (EtOH treated) the immunofluorescence images (Fig. 4a, c, e) show a typical accumulation of the protein in the perinuclear region (presumably Golgi apparatus) as observed for HA-tagged APP WT (Fig. 3). Similarly, as described for the APP cysteine mutants, we determined the changes in subcellular localization of inducible dimerized APP. For quantification of

APP dimers in the ER (Fig. 4a), Pearson correlation coefficient was used to measure the linear correlation between the intensity of the APP (monomer or dimer) signal and its signal intensity co-localized with the ER marker (KDEL-mRFP). The quantification shows an increase for dimerized APP in the ER (Fig. 4b). Quantification of immunofluorescence images of non-treated control cells (EtOH, APP F1 and APP F2) shows that monomeric APP is highly co-localized with the *cis*-Golgi marker GM130 (Fig. 4c). This co-localization is strongly reduced when dimerization of APP F1 and APP F2 was induced (APP F1, $p = 0.004$; APP F2, $p = 0.022$) (Fig. 4c, d). In contrast, analysis of monomeric versus dimeric APP localization in early endosomes revealed that induced dimerization leads to an accumulation of APP in this compartment (Fig. 4e). Again, significance levels were only reached for APP F2 (unpaired Student's t test, $p = 0.013$) (Fig. 4f). Although both, APP F1 and APP F2 signals were clearly altered, significance levels were reached in case of ER and endosomes only for APP F2 (unpaired Student's t test, $p = 0.037$), likely, because the extent of APP F2 dimerization is more pronounced. Quantitative analysis of monomeric (EtOH treated control) and dimeric APP co-localized with lysosomes (marker: LAMP1) revealed no significant differences (Fig. S2).

Taken together, APP dimerization leads to an accumulation of APP in the ER, a strong reduction in the *cis*-Golgi compartment and to an accumulation in early endosomes while lysosomal levels were essentially unchanged.

APP levels are decreased at the cell surface after induced dimerization

It has been shown that APP forms homo-dimers at the cell surface [22]. To test, if dimerization might affect the amount of APP at the plasma membrane, we labeled cell surface APP F1 in its monomeric and dimeric state in non-permeabilized cells (Fig. 5a). Cell surface staining of APP was confirmed with the cell surface marker IL2 td tomato (Fig. S3) [31]. Quantification of these stainings revealed a significant decrease of APP F1 dimers at the cell surface, when compared to control APP F1 (EtOH) of about twofold (Fig. 5b; 50 ± 4%, unpaired Student's t test, $p < 0.001$).

Also, quantitative analysis of cell surface stainings of constitutive APP dimers (cysteine mutants) in comparison to APP WT showed a significant reduction for both APP cysteine mutants L17C (27.0 ± 6.9%) and K28C (24.1 ± 5.0%) in the percentage of cell surface constituent APP dimers (Fig. 5d). The data obtained with immunostainings were confirmed via cell surface biotinylation (Fig. S4).

Together these data indicate that elevated APP dimerization causes a decrease of APP levels at the cell surface.

Internalization rate of APP is not affected by dimerization

Our data demonstrate an increase of dimerized APP in endosomes and a decrease of cell surface APP dimers. To analyze if this might be a consequence of a higher endocytosis rate of dimerized APP, an antibody uptake assay was performed. To allow direct comparison of the different APP mutants, we used N-terminally c-myc-tagged constructs and tested for anti-c-myc antibody uptake. For constitutive dimerization of APP (cysteine mutants), here only myc-APP L17C was used. In addition, an endocytosis-impaired myc-APP construct lacking the NPTY motif (APPΔNPTY) was included as a negative control [43].

Cells expressing N-terminally c-myc-tagged APP WT, APPΔNPTY, APP L17C, and APP F1 in the monomeric (EtOH) and dimerized state were incubated at 4 °C and cell surface APP was loaded with anti-c-myc antibodies. After 1 h, unbound anti-c-myc antibody was removed and endocytosis was allowed by incubating the cells at 37 °C. Then the cells were fixed after 5, 10, and 15 min. Residual surface-exposed APP was visualized by staining of non-permeabilized cells with fluorescence-labeled secondary antibodies. Afterwards, cells were permeabilized and stained with a different secondary antibody to visualize endocytosed APP. The assay was quantified by analysis of the signal intensity of endocytosed APP versus cell surface APP. Representative images of APP after the different incubation time points at 37 °C are shown in Fig. 6a. Quantification of the data revealed only at one time point, 10 min after induced endocytosis, a slight but significant increase for dimerized APP F1 compared to the APP F1 control (13.5 ± 2.5%, unpaired Student's t test, $p < 0.001$) (Fig. 6b). Similarly, APP L17C also showed a significant increase in the internalization rate after 10 min compared to APP WT (5 ± 1.6%, one-way ANOVA with Tukey's HSD post hoc test, $p < 0.05$). In contrast, endocytosis of APPΔNPTY was reduced at the 10 and 15 min time points about 30%, as observed before [34].

Taken together, we conclude that the observed change in the antibody uptake assay at only one time point does not point towards a robust change in the endocytosis rate upon dimerization.

Induced APP dimerization leads to decreased sAPPα and sAPPβ levels

In our previous study we showed that APP L17C and APP K28C are not suitable for analysis of APP processing, as mutations at these sites affect APP cleavage independent of its dimerization status. However, using the controlled homodimerization of APP–FKBP assay, we observed a 50% reduction in total Aβ levels in N2a cells, which were mainly due to γ-secretase inhibition [24]. Interestingly, we

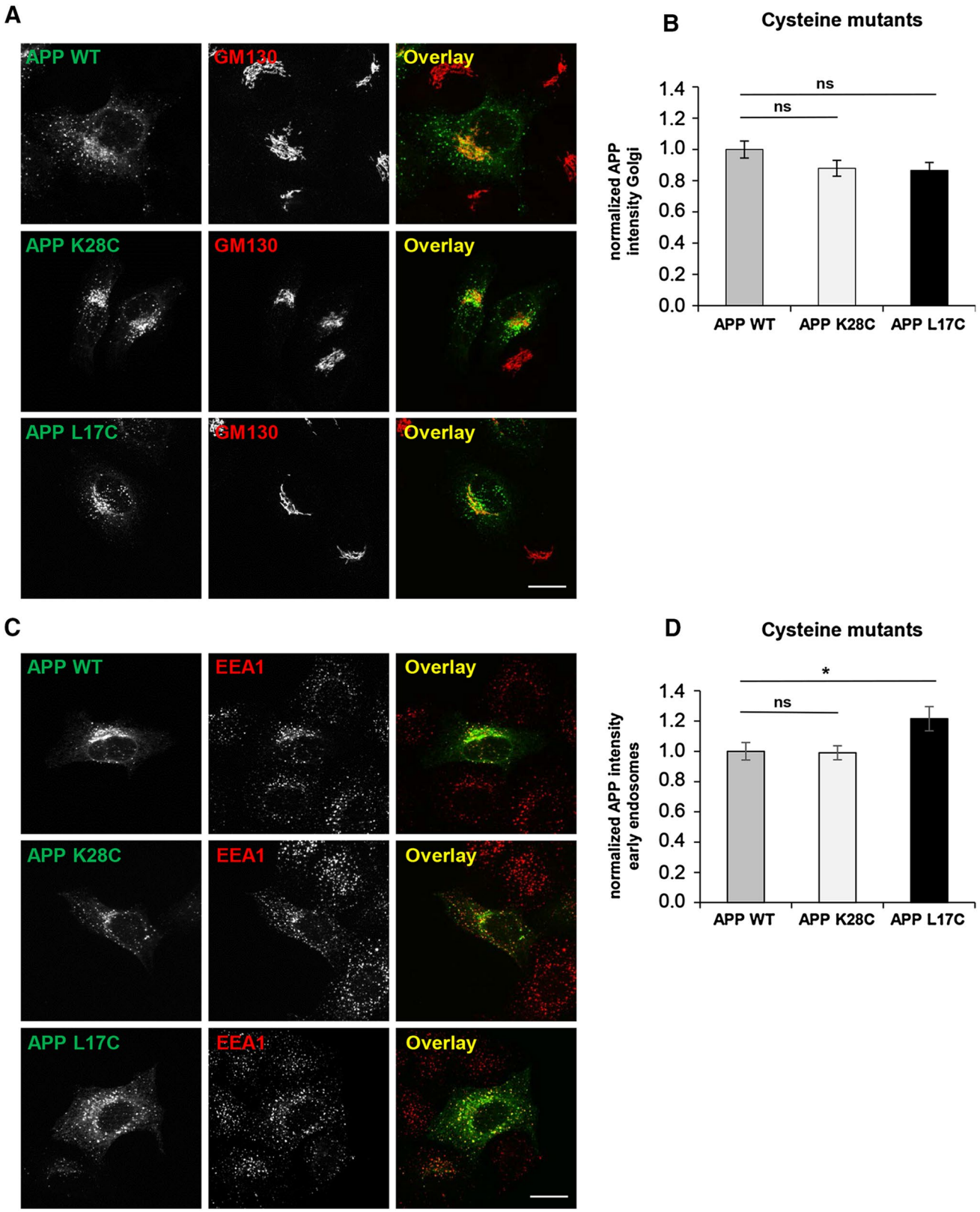

also observed a decrease in sAPP levels, which has not been analyzed in detail in this previous study. To address the question, if controlled induced dimerization leads to changes in sAPP production, we now analyzed sAPPα and sAPPβ levels after induced dimerization of APP F1 with two different concentrations of dimerizer (50 and 100 nM) in transiently

◂**Fig. 3** Localization of APP K28C and L17C after constitutive dimerization in the *cis*-Golgi and in endosomes. **a** HeLa cells expressing N-terminally HA-tagged APP WT and APP K28C and L17C were double-immunostained with α-HA (*green*) and α-GM130 (*red*, *cis*-Golgi marker) antibodies or **c** α-HA (*green*) and α-EEA1 (*red*, early endosomal marker) antibodies. **b** Quantification of APP WT, K28C, and L17C in the *cis*-Golgi apparatus. **d** Quantification of APP WT, K28C, and L17C in early endosomes. *Bars* represent mean values ± SEM; APP WT ($n = 38/N = 4$), APP K28C ($n = 50/N = 4$), APP L17C ($n = 53/N = 4$) unpaired Student's t test, $^{*}p < 0.05$, $^{**}p < 0.01$, $^{***}p < 0.001$. *Scale bar* 10 µm

transfected cells overnight. Equal amounts of cell lysates and conditioned cell media were separated via SDS-PAGE and analyzed via Western Blot. Quantification of secreted fragments versus full-length APP revealed a significant reduction of proteolytic conversion of dimerized APP F1 by α- and β-secretases (Fig. 7a, b).

APP shows reduced binding to LRP1 after induced dimerization

We assumed that alterations of APP dimer localization might be explained by changes in its interaction with different sorting molecules. To address this point, we analyzed the APP monomer/dimer interaction with different known APP sorting molecules. As previously reported, one of these proteins is the type I transmembrane protein SorLA (sorting protein-related receptor with A-type repeats), also known as LR11/SORL1 [44], which is assumed to prevent APP dimer formation [45]. We tested two further members of the Vps10p (vacuolar protein sorting 10 protein) domain receptor family, SorCS1cα and Sortilin, which were both shown to interact with APP and to influence APP transport [31, 46–48] as well as LRP1 which is known to interact with APP via Fe65 [14, 49, 50].

Co-immunoprecipitation studies were performed with HeLa cells expressing non-dimerized or dimerized HA-tagged APP F1 together with either SorLA, RFP-tagged Sortilin or Venus-tagged SorCS1cα by pull down of APP via anti-HA-coupled beads. No differences in the signal intensity of SorLA (Fig. 8d), SorCS1cα (Fig. 8e), or Sortilin (Fig. 8f) were observed between control cells (EtOH)-expressing monomeric APP F1 and those cells where dimerization of APP F1 was induced (AP20187). In contrast, the levels of co-immunoprecipitated LRP1 were significantly lower after induced dimerization of APP (Fig. 8g), which was confirmed by densitometric measurements and statistical analysis of signal intensities (Fig. 8c).

Together these data show a significantly decreased APP–LRP1 interaction after increasing APP dimerization, while binding to three members of the Vps10p domain receptor family, SorLA, SorCS1cα and Sortilin, was unaffected.

APP dimerization lowers the rate of APP and SorLA co-transport in retrogradely transported membrane organelles

APP and SorLA showed a high degree of co-localization in endosomes and the Golgi apparatus (Fig. S5), two compartments, where we observed the most pronounced alterations in APP localization after dimerization. Therefore, we analyzed the influence of APP dimerization on SorLA co-localization in more detail. Using time-lapse imaging we evaluated transport characteristics of APP GFP, APP F1 GFP, and SorLA RFP in primary cortical mouse neurons (DIV6). We observed that the velocity profile of anterograde- and retrograde-transported monomeric and dimeric APP GFP vesicles was mostly unaffected after co-expression with SorLA (Fig. 9a–d). Only retrograde APP dimer transport was significantly increased for vesicles with a velocity between 1.5 and 2 µm/s, but the mean velocity remained unchanged (Fig. S6). Notably, monomeric and dimeric APP showed neither a difference in their mean velocities nor in the relative amount of anterograde, retrograde, and stationary vesicles (Fig. 9f; Fig. S6). However, co-expression of SorLA led to a significant decrease of stationary vesicles and a clear increase in retrograde APP transport, more pronounced for dimerized APP (Fig. 9e–h). Similarly, APP co-expression caused a decrease of SorLA bearing stationary vesicles (Fig. 9g). Notably, the percentage of vesicles, co-transporting APP and SorLA is only about 10% (Fig. 9h). Analysis of the relative amount of SorLA co-transported in APP vesicles per µm did not reveal any changes in anterograde transport. However, for retrograde transport, APP dimerization caused a significant reduction of APP/SorLA co-transport (Fig. 9h).

Together, these data show that SorLA induces mobilization of APP retrograde transport and that APP dimerization reduces its co-transport rate with SorLA. Therefore, we conclude that reduced co-transport of SorLA with dimerized APP might indeed be responsible for the increased levels of dimerized APP in endosomes.

Discussion

APP can form homomeric complexes, as demonstrated by different groups with a variety of different methods [22–25, 27, 42, 51]. Several studies suggested that APP dimers exist in different subcellular compartments, including ER, Golgi, and the plasma membrane [22, 27, 28]. Now we show in more detail that forced APP dimerization alters its subcellular localization (Fig. 10), likely by altering the interaction with different sorting molecules, including SorLA and LRP1.

APP dimers were reported to be formed as early as in the endoplasmic reticulum (ER) [25, 27, 28]. We observed

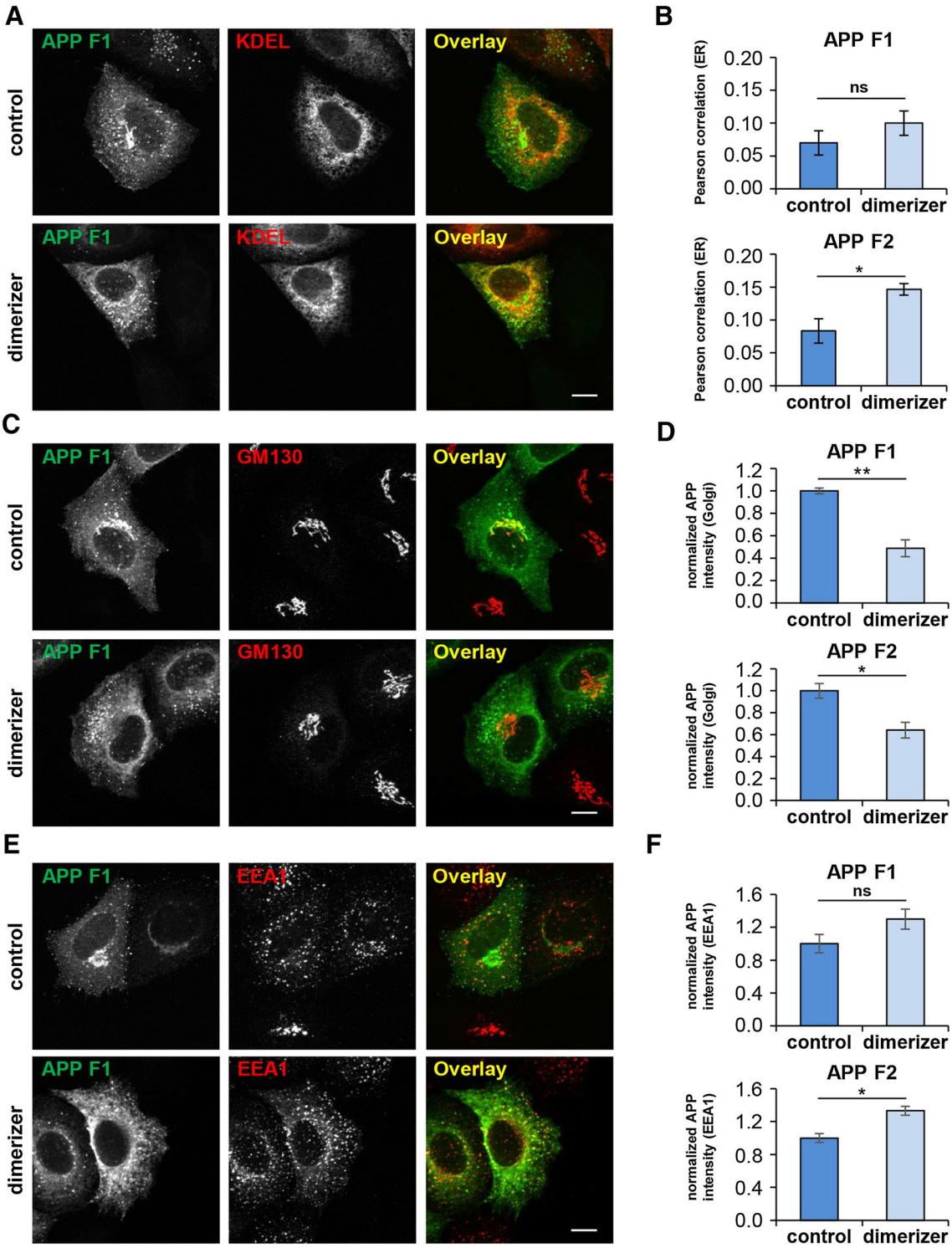

APP dimers in this compartment as well and our quantitative comparable analysis revealed that APP dimerization causes an accumulation of APP in the ER (Fig. 4). This suggests that APP monomers are preferentially transported from the ER to the Golgi.

Predominant localization of APP monomers in the Golgi apparatus has been demonstrated in earlier studies and is in

◂**Fig. 4** Localization of APP F1 and APP F2 after induced dimerization in the ER, *cis*-Golgi, and endosomes. HeLa cells expressing C-terminally HA-tagged APP F1 or APP F2 were treated for 1 h with 100 nM AP20187 to induce dimerization. As a control the same volume of the vehicle EtOH was added. For analysis of subcellular localization, APP F1 (**a**, **c**, **e**) and APP F2 (not shown) were immunolabelled with an α-HA antibody (*green*). **a** APP F1 localization in the ER was determined by co-localization with exogenously expressed KDEL-mRFP (*red*). **c**, **e** APP F1 localization in the *cis*-Golgi and in endosomes was determined by co-immunolabelling with α-GM130 (*red*) and α-EEA1 (*red*) antibodies, respectively. Co-localization is indicated in *yellow* (overlay). **b**, **d**, **f** Quantification of non-dimerized and dimerized APP F1 and APP F2 intensities within the ER, *cis*-Golgi and endosomes were determined using CellProfiler 2.1.0. For **b** ER the Pearson correlation coefficient and for **d**, **f** *cis*-Golgi and endosomes an object-based analysis was used (APP F1: increase in the ER: 56.9 ± 21.6%, decrease in Golgi 55.3 ± 7.8%, increase in endosomes 30.5 ± 3.4%; APP F2: increase 89.7 ± 33.7%, decrease in Golgi 36.2 ± 2.8%, increase in endosomes 33.3 ± 1.7%). *Bars* represent mean values ± SEM; ($n > 12/N = 3$); unpaired Student's *t* test, $^{*}p < 0.05$, $^{**}p < 0.01$, $^{***}p < 0.001$. *Scale bar* 10 µm

line with our results [52–54] (Fig. 4). Further, it had been qualitatively shown that APP dimers co-localize to a lower extent with the *trans*-Golgi network marker TGN46 [28]. This finding was now validated by our data, indicating a significant reduction in the signal of APP F1 and APP F2 dimers (55.3 and 36.2%, respectively) in the *cis*-Golgi apparatus (Fig. 4). This might be explained by retention of APP dimers in the ER. However, as assumed by others before, APP dimerization might also promote APP anterograde transport towards the plasma membrane or to endosomal compartments [28]. Latter assumption is further supported by our data, showing that APP dimerization was accompanied with an increased localization to early endosomes (Figs. 3, 4). Consistently, it has been reported that copper, favoring APP dimerization [40, 55], promotes redistribution of APP from a perinuclear location to a more peripheral distribution in the cell, including localization to early endosomes [56].

It has been reported before that a small amount of APP homo-dimers is localized at the cell surface [22]. We also observed dimerized APP at the cell surface but interestingly we found that APP dimerization causes a decrease of APP at the plasma membrane (Fig. 5). We speculated that APP dimerization might promote APP endocytosis as published for other cell surface receptors like EGF (epidermal growth factor) receptor, PDGF (platelet-derived growth factor) receptor, NGF (nerve growth factor) receptor or HGF (hepatocyte growth factor) receptor [57–59]. Indeed, after induction of dimerization we observed an increase in early steps of APP endocytosis (Fig. 6). As the difference in internalization was not very pronounced, we assumed that decreased APP dimer localization at the plasma membrane is not only explained by an increased endocytosis rate, but likely also results from reduced anterograde trafficking of dimeric APP to the cell surface.

Finally, we found an accumulation of APP dimers in endosomes (Figs. 3, 4). We suppose that this is either a consequence of its direct exit from the Golgi apparatus and/or is caused by its increased internalization by the plasma membrane. Moreover, it has been reported that APP dimers do not co-localize with the established recycling endosomal marker TfR (transferrin receptor) [28]. Thus, reduced trafficking of APP dimers to recycling endosomes might also contribute to APP dimer accumulation in endosomes. Notably, impaired entering of APP dimers in the recycling pathway might also add on to the observed decrease of surface APP after dimerization. Theoretically, the increase of dimerized APP in endosomes could also result from decreased transport to late endosomes and lysosomes. However, we did not observe any accumulation of APP dimers in LAMP1-positive vesicles, arguing against this possibility.

Why does APP dimerization cause a change in APP localization? We assumed that APP dimerization affects binding to sorting receptors. To test this hypothesis we analyzed three members of the Vps10p domain receptor family, SorLA, SorCS1cα, and Sortilin, all known to interact with APP mainly via the ectodomain [31, 44, 48] and to influence APP transport at different angles of the secretory pathway. SorLA is known to be involved in retrograde transport of APP from endosomes to the TGN [14]. Sortilin is located predominantly in the TGN and cycles between endosomes and TGN similarly as SorLA, but seems to shuttle APP mainly in anterograde direction to early endosomes and then to the cell surface [48, 60]. Sortilin is also known as an endocytic receptor, which internalizes various ligands by receptor-mediated endocytosis and delivers them to lysosomes [37]. SorCS1cα, an endocytic receptor, was shown to reduce the anterograde transport rate of APP [31]. After induced dimerization of APP followed by Co-IP, neither SorLA, SorCS1cα, nor Sortilin levels were changed (Fig. 8). This suggests that the status of APP dimers does not affect interaction with these sorting receptors. However, as binding of APP to these proteins might only be transient, changes between these interacting molecules can be easily overseen in co-immunoprecipitation experiments. Moreover, as we were using an inducible dimerization system, we cannot exclude that thereby indirect influences of SorLA on APP

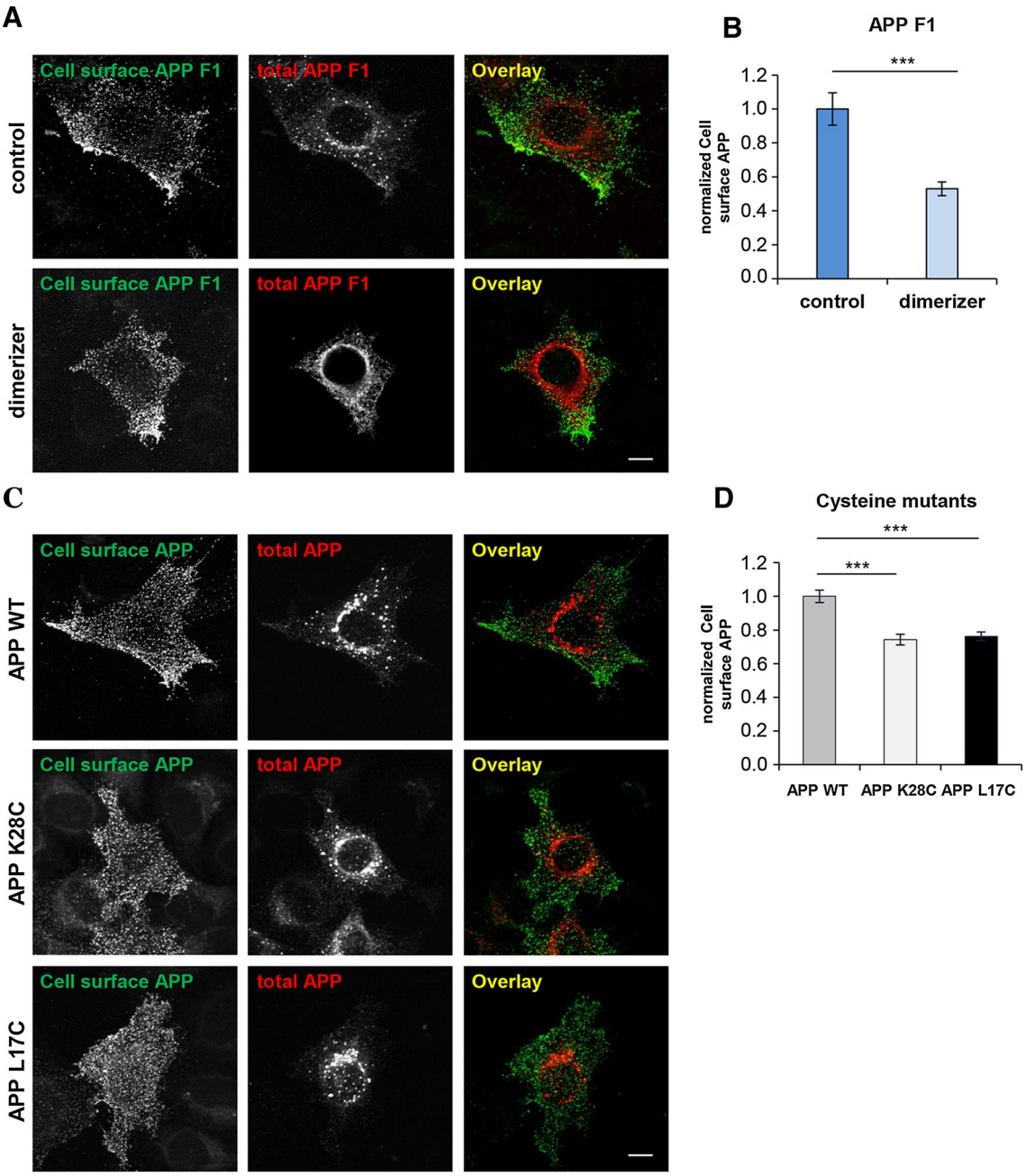

Fig. 5 Analysis of cell surface and intracellular APP monomers/dimers. **a**, **b** HeLa cells expressing N-terminally HA-tagged APP F1 were incubated for 1 h with 100 nM AP20187 to induce dimerization. As a control, the treatment was carried out with the same volume of the solvent EtOH. **a** The cells were subsequently subjected for intracellular (permeabilized cells) and cell surface (non-permeabilized cells) stainings using α-HA antibody combined with different secondary antibodies (surface: Alexa Fluor-488, *green*; intracellular: Alexa Fluor-594, *red*). The overlay shows relative intensities of total (*red*) and cell surface (*green*) APP. **b** Quantification of the percentage (%) of cell surface APP after induced dimerization using CellProfiler 2.1.0. Note the significant decrease (49.8 ± 3.9%) of dimerized surface APP. **c**, **d** HeLa cells expressing N-terminally HA-tagged APP WT, APP L17C or APP K28C were subjected to total and cell surface stainings using α-HA antibody combined with different secondary antibodies as described above. **d** Quantification of the percentage (%) of cell surface APP WT and APP cysteine mutants using CellProfiler 2.1.0. For both cysteine mutants a significant decrease (L17C, 27.0 ± 6.9%; K28C, 24.1 ± 5.0%) of surface APP was observed. *Bars* mean values ± SEM; ($n > 13/N = 3$); unpaired Student's *t* test, $*p < 0.05$, $**p < 0.01$, $***p < 0.001$. *Scale bar* 10 µm

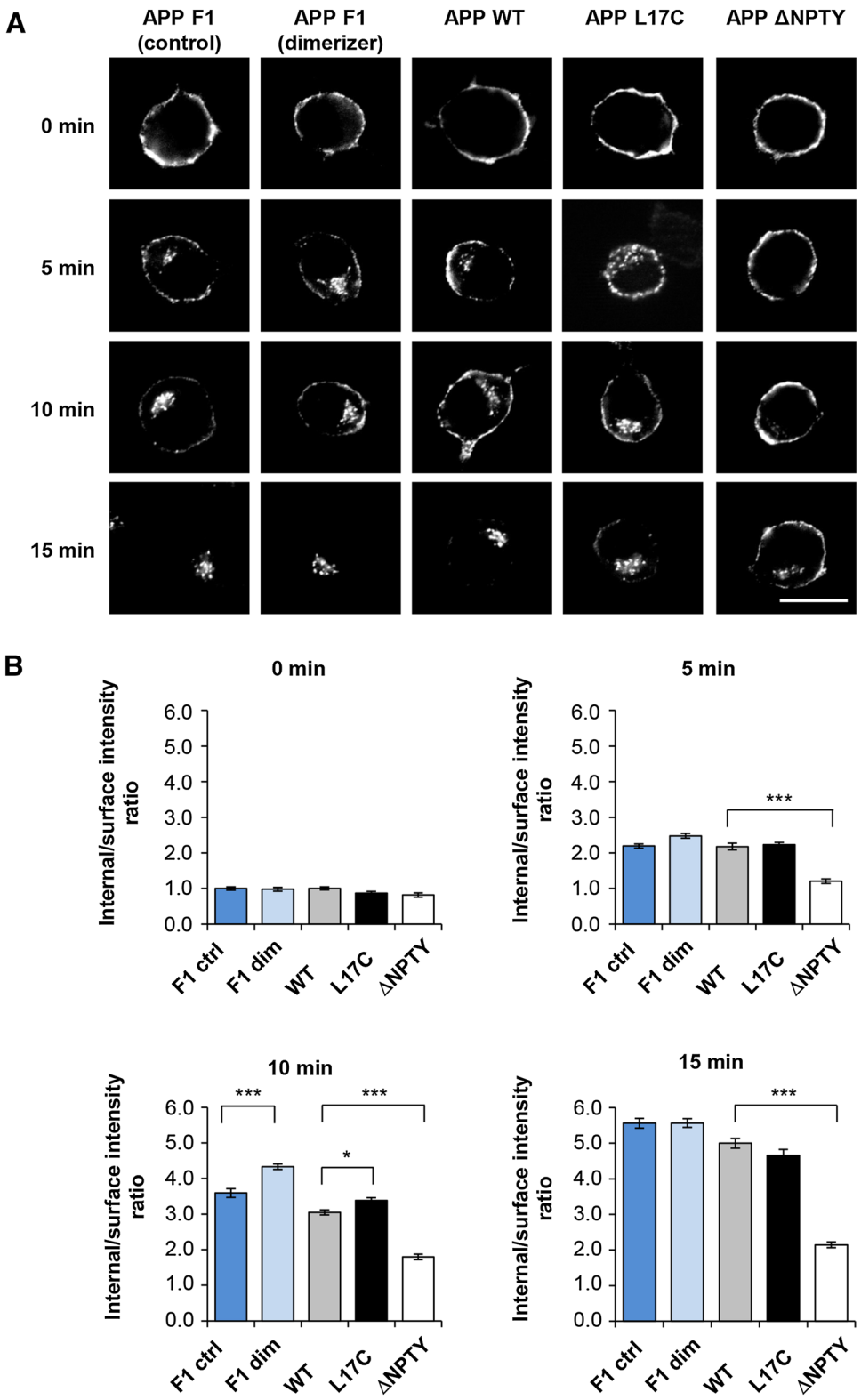

Fig. 6 Analysis of endocytosed APP F1 and APP cysteine mutants. **a** Immunofluorescence images of N2a cells transiently transfected with N-terminally c-myc-tagged APP WT, APP F1, APP L17C, and APP ΔNPTY. For the APP F1 construct, dimerization was induced for 1 h with 100 nM AP20187 and as a control, the same volume of the solvent EtOH was added. An antibody uptake assay was performed, following antibody endocytosis at four different time points (0, 5, 10, and 15 min). Immunolabelling was carried out with α-c-myc antibody for cell surface APP at 4 °C. Then cells were allowed to endocytose antibody-labeled APP for 5, 10, and 15 min at 37 °C. After fixation, non-permeabilized cells were stained with a secondary antibody (Alexa Fluor-488) to visualize surface APP. Afterwards cells were permeabilized and the endocytosed APP antibody complex was labeled with a secondary antibody (Alexa Fluor-594). Here, only the signal of Alexa Fluor-594 is shown, representing endocytosed APP and to a minor extent also cell surface APP not blocked by binding of the Alexa Fluor-488 antibody. *Scale bar* 10 µm. **b** Internal/total intensity ratio of densitometric measurements for all target proteins used at the different endocytosis time points. *F1 dim* APP F1 treated with dimerizer, *F1 ctrl* APP F1 treated with ethanol, *WT* APP wild type, *L17C* APP carrying an L17C mutation, *ΔNPTY* APP lacking the NPTY motif. *Bars* mean values ± SEM; ($n > 15/N = 3$); one-way ANOVA with Tukey's HSD post hoc test *$p < 0.05$, **$p < 0.01$, ***$p < 0.001$

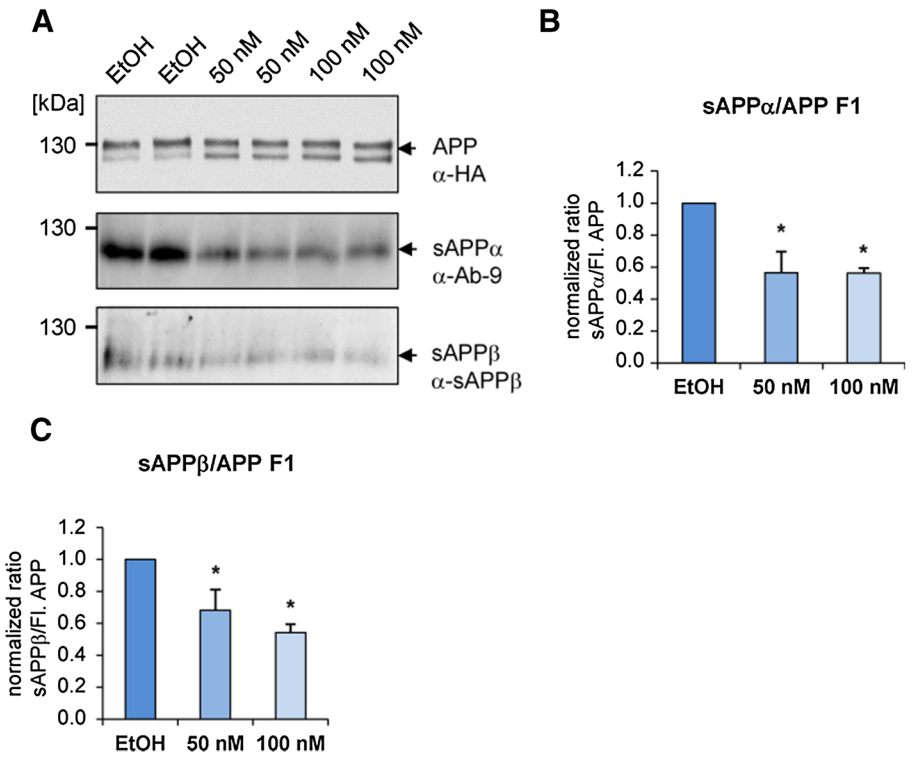

Fig. 7 Analysis of sAPPα and sAPPβ after controlled dimerization of APP. N2a cells expressing APP F1 were treated overnight with dimerizer (50 and 100 nM or the solvent ethanol as a control). **a** Western blot analysis of cell lysates was carried out using α-HA antibody to detect full-length APP and of conditioned medium using Ab-9 directed against sAPPα and anti-sAPPβ, the different secreted fragments. Quantification of densitometric measurements of sAPPα/full-length APP (**b**) and sAPPβ/full-length APP (**c**). *Bars* mean values ± SEM; $n = 3$, one-way ANOVA with Tukey's HSD post hoc test $^{*}p < 0.05$, $^{**}p < 0.01$, $^{***}p < 0.001$

dimers are not exerted. Therefore, we investigated the trafficking of monomeric and dimeric APP in interplay with sorting proteins in more detail.

Since it was shown that SorLA affects APP trafficking from endosomes to the TGN [14] and the fact that we found a decrease of APP dimers in the Golgi and an increase in early endosomes, we concentrated our study on this receptor. Indeed, our time-lapse imaging data indicated that dimerization of APP led to reduced co-transport of APP with SorLA in retrograde, but not in anterograde transport vesicles (Fig. 9). Thus, the reduction of dimerized APP in the Golgi and the increase in endosomes might result from altered sorting of APP in its monomeric or dimeric state by SorLA. In line with those results, a report from Willnow and colleagues showed a strong increase of APP dimers in brains of SorLA KO mice, underlining an interplay of SorLA and APP dimerization [45].

Besides the above-discussed members of the Vps10p domain receptor family, APP trafficking is also affected by a family member of the related LDL-related receptors, LRP1 [49, 61]. Interestingly, we found decreased LRP1 binding to dimerized APP in the Co-IP assay (Fig. 8). Thus, APP dimerization might impair the interaction with LRP1 and in turn affect its trafficking. Based on current knowledge, reduced binding of APP dimers to LRP1 is expected to increase its anterograde transport to the plasma membrane [14, 50]. Thus, it appears reasonable that the decrease of dimerized APP in the Golgi apparatus is explained by reduced binding of APP dimers to LRP1. However, additional factors, including different APP C-terminal interaction partners, such as Calsyntenin1, X11 or Fe65 which affect APP localization might also contribute [62–66]. For example, Fe65 binds to both the C terminus of APP and the C terminus of LRP1 and functions as a link between these

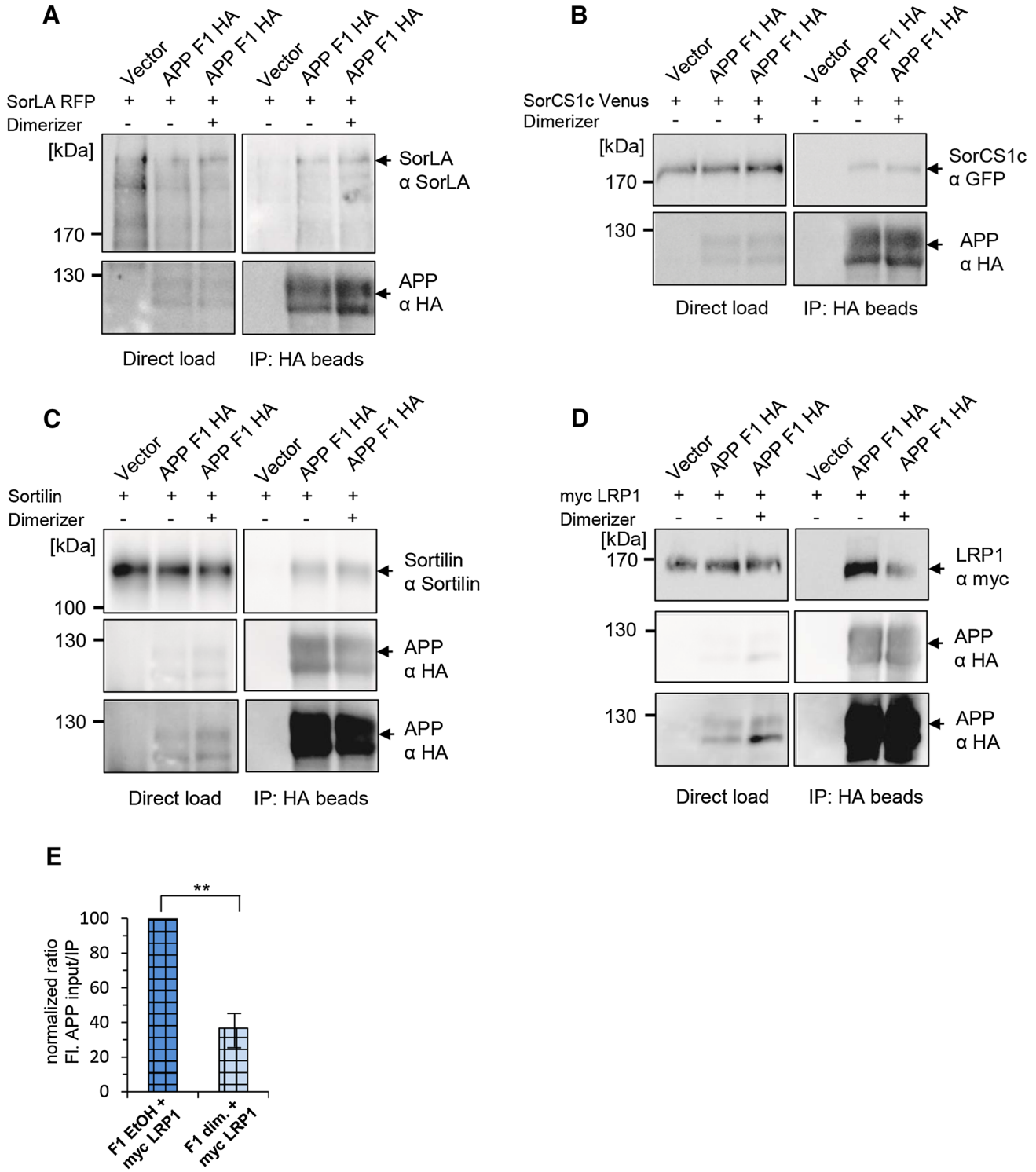

Fig. 8 Co-immunoprecipitation of APP and SorLA, SorCS1cα, Sortilin, and LRP1 after controlled dimerization of APP. HeLa cells were transiently co-transfected with C-terminally HA-tagged APP F1 constructs and SorLA RFP (**a**) or SorCS1cα Venus (**b**), Sortilin (**c**) or myc LRP1 CT (**d**). HeLa cells transfected with SorLA RFP (**a**), SorCS1cα Venus (**b**), Sortilin (**c**), and myc LRP1 (**d**) constructs and empty vector served as negative controls. Equal amounts of cell lysates were loaded directly on an SDS gel and analyzed via western blot with primary α-HA antibody. Further, equal amounts of cell lysates were used for immunoprecipitation with α-HA antibody-coated agarose beads. The samples were separated on an SDS gel and subjected for western blot detection with the primary antibodies α-SorLA (SorLA), α-GFP (SorCS1cα Venus), α-Sortilin (Sortilin), and α-c-myc (myc LRP1). The same membrane was incubated afterwards with anti-HA antibody to detect total amounts of immunoprecipitated APP ($n = 4$ for Co-IP with LRP1 and SorLA, $n = 2$ for Co-IP with SorCS1cα and Sortilin). **e** Quantification of data shown in D (APP F1–myc LRP1 interaction). *Bars* represent mean values ± SEM; $n = 4$, unpaired Student's t test $^{*}p < 0.05$, $^{**}p < 0.01$, $^{***}p < 0.001$

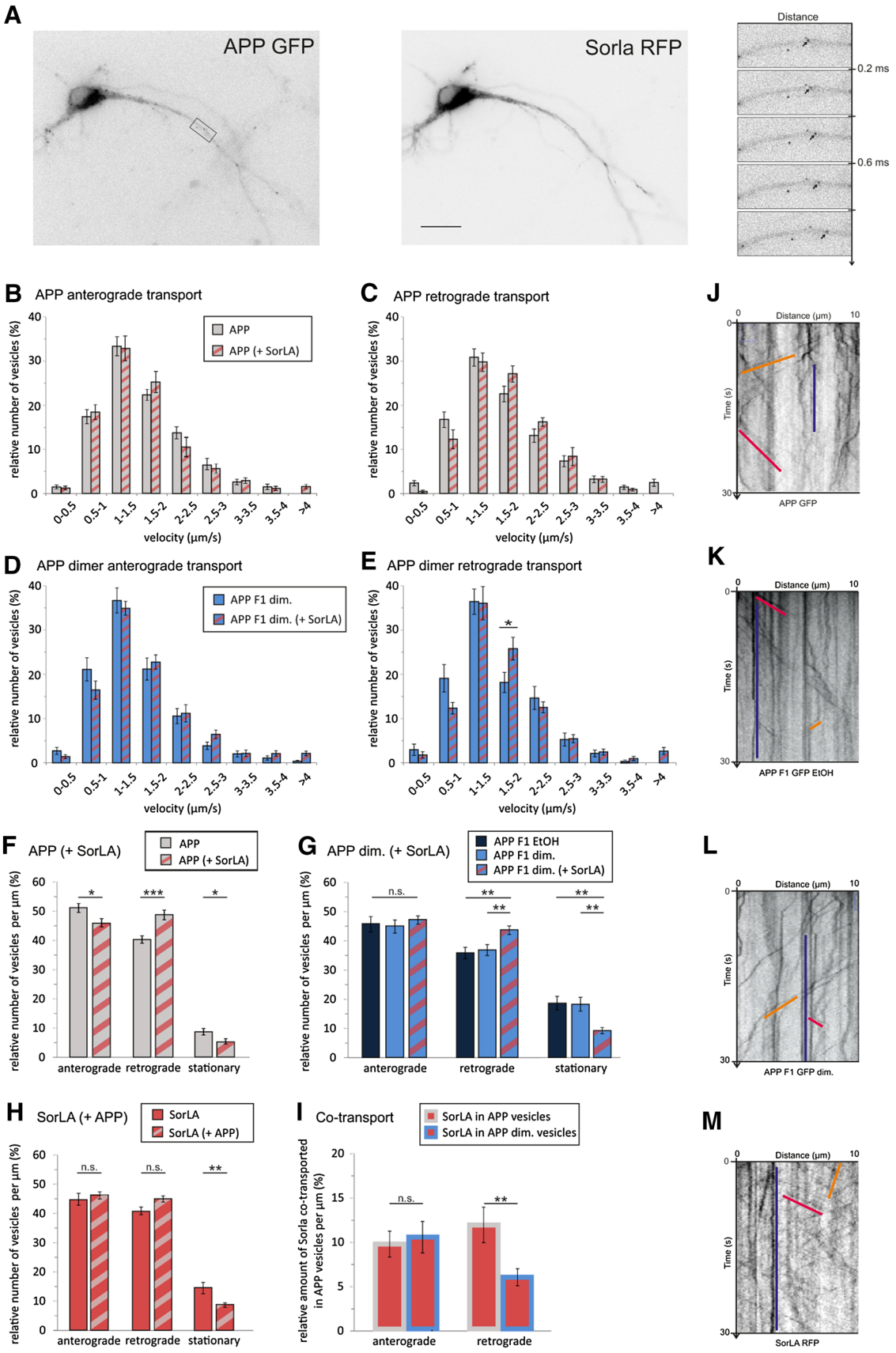
A
APP GFP
Sorla RFP
Distance
0.2 ms
0.6 ms
B APP anterograde transport
APP
APP (+ SorLA)
relative number of vesicles (%)
velocity (µm/s)
C APP retrograde transport
J
Distance (µm)
Time (s)
APP GFP
D APP dimer anterograde transport
APP F1 dim.
APP F1 dim. (+ SorLA)
E APP dimer retrograde transport
K
APP F1 GFP EtOH
F APP (+ SorLA)
relative number of vesicles per µm (%)
anterograde
retrograde
stationary
G APP dim. (+ SorLA)
APP F1 EtOH
APP F1 dim.
APP F1 dim. (+ SorLA)
n.s.
L
APP F1 GFP dim.
H SorLA (+ APP)
SorLA
SorLA (+ APP)
I Co-transport
SorLA in APP vesicles
SorLA in APP dim. vesicles
relative amount of Sorla co-transported in APP vesicles per µm (%)
M
SorLA RFP

◂**Fig. 9** Live cell recordings of APP and SorLA after controlled dimerization of APP. Primary cortical mouse neurons were transfected at DIV5 via calcium phosphate to analyze transport of APP GFP, APP F1 GFP, and SorLA RFP after 18–20 h at DIV6. Examples of transiently co-transfected neurons are depicted in **a**. Analysis of **b** anterograde and **c** retrograde transport of APP GFP only and after co-expression with SorLA RFP. Histogram showing quantification of the number of recorded vesicles moving at velocities between 0.05 and 4 µm/s. *Bars* mean values ± SEM ($n = 19/N = 3$ for APP GFP, $n = 14/N = 3$ for APP GFP + SorLA RFP). Analysis of **d** anterograde and **e** retrograde transport of dimerized APP F1 GFP only and after co-transfection with SorLA RFP. Histogram showing quantification of the number of recorded vesicles moving at velocities between 0.05 and 4 µm/s. *Bars* represent mean values ± SEM; ($n = 20/N = 3$ for APP F1 GFP dimerized, $n = 15/N = 3$ for APP F1 GFP dimerized + SorLA RFP). **f**, **g** Relative number of vesicles per µm showing the percentage of anterograde, retrograde, and stationary vesicles for APP GFP only and after co-transfection with SorLA RFP ($n = 19/N = 3$ for APP GFP) ($n = 14/N = 3$ for APP GFP + SorLA RFP). APP F1 GFP (vehicle EtOH/dimerized) only and APP F1 GFP dimerized after co-transfection with SorLA. *Bars* mean values ± SEM; ($n = 16/N = 3$ for APP F1 GFP EtOH, $n = 20/N = 3$ for APP F1 GFP dimerized, $n = 15/N = 3$ for APP F1 GFP + SorLA RFP). **h** Relative number of vesicles per µm showing the percentage of anterograde, retrograde, and stationary vesicles for SorLA RFP only and after co-transfection with APP GFP ($n = 19/N = 3$ SorLA RFP, $n = 14/N = 3$ for APP GFP + SorLA RFP). **i** Relative amount of SorLA co-transported in APP vesicles per µm (%). *Bars* mean values ± SEM; ($n = 14/N = 3$ for APP GFP + SorLA RFP, $n = 15/N = 3$ for APP F1 GFP + SorLA RFP), two-way ANOVA $^{*}p < 0.05$, $^{**}p < 0.01$, $^{***}p < 0.001$. Representative kymographs of cells expressing (**i**) APP GFP (**j**) APP F1 GFP (EtOH) (**j**) APP F1 GFP (dimerizer) (**k**) SorLA RFP. Anterograde transport is defined as an angle of <90° (*red line*), retrograde transport as an angle of >90° (*orange line*), and stationary vesicles are visible parallel to the time axis (*blue line*)

two receptors [67]. In line with this, a recent study using a split-luciferase system reported that APP dimerization was increased when they used a construct lacking the APP C terminus (APP ΔCT), implicating the APP C terminus in regulating APP dimerization [51].

We observed an accumulation of APP in its dimeric state in endosomes (Figs. 2, 3, 4). Due to increased activity of BACE in endosomes [3], an elevated Aβ production and increased sAPPβ generation is expected. However, we have shown previously using the FKBP-based dimerization system that induced APP dimerization causes a decrease in Aβ generation [24] and show in this manuscript reduced sAPPβ production after induced dimerization (Fig. 6). It is clear that the amyloidogenic secretases (β and γ) are able to process APP in its monomeric and dimeric form [26, 68, 69], but monomeric/dimeric APP might differ in substrate preferences for α- and/or β-secretase. In line with this, inhibition of γ-secretase cleavage by APP dimerization was also suggested by other studies [70–72]. A similar mechanism might also hold true for BACE1. Accordingly, studies of SorLA knockdown cells, assumed to express elevated APP dimers, reported altered substrate affinities for APP monomers and dimers [45]. Moreover, BACE1 itself can dimerize in its active state [73, 74]. However, alternatively in our experiments, the decreased generation of sAPP might be explained by reduced APP surface levels. In this context it is also interesting to note that different γ-secretase complexes, including PS1 or PS2, were reported to be active at the plasma membrane, TGN, and endosomes [75, 76]. Thus, future experiments addressing the affinities of those complexes to APP in its monomeric or dimeric form could help to solve some of the contradictory data addressing Aβ generation.

Taken together, our data suggest that forced APP dimerization affects its subcellular localization, likely by altering the trafficking by SorLA and/or LRP1. This in turn influences sAPPα, sAPPβ, and Aβ generation, underlining the importance of the regulation of the APP dimerization state. Thus, future experiments, elucidating factors, such as copper or heparin, modulating APP dimerization might open novel avenues for development of pharmacological strategies preventing development of AD.

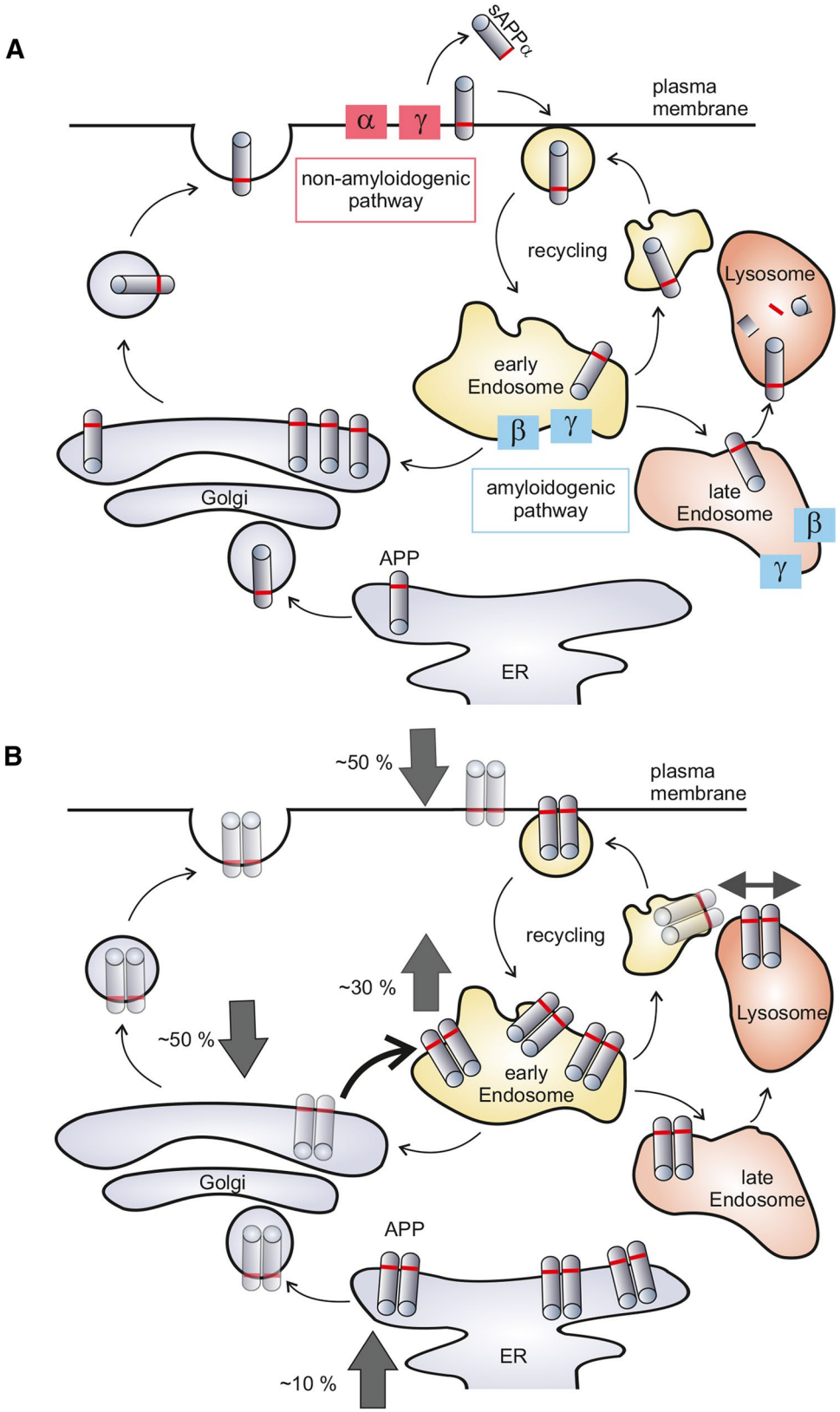
A
sAPPα
plasma membrane
α
γ
non-amyloidogenic pathway
recycling
Lysosome
early Endosome
β
γ
amyloidogenic pathway
late Endosome
β
γ
Golgi
APP
ER
B
~50 %
plasma membrane
recycling
~30 %
~50 %
Lysosome
early Endosome
Golgi
late Endosome
APP
ER
~10 %

◂**Fig. 10** APP dimerization alters its localization. **a** Model of APP trafficking and processing in different cellular compartments. Under physiological conditions, APP is mainly present in its monomeric form and travels the secretory pathway (*gray*) from the ER to the plasma membrane via the Golgi apparatus, where it is predominantly localized. From the plasma membrane, APP enters the endocytic recycling pathway via early endosomes (*yellow*) from where it is further sorted: either back to the cell surface, or back to the TGN in a retromer-mediated pathway, or trafficked to late endosomes which fuse to lysosomes where APP is degraded (*orange*). Note that non-amyloidogenic processing by α- and γ-secretases predominantly takes place at the plasma membrane while amyloidogenic processing of APP by β- and γ-secretases is mostly carried out in early and late endosomes. **b** Sorting of APP dimers: Forced APP dimerization causes an accumulation in the ER and in endosomes and results in decreased localization to the Golgi apparatus and the plasma membrane. Levels in lysosomes remained unchanged. The altered localization of APP dimers is likely explained by changes in the interaction with sorting molecules such as SorLA and LRP1

Acknowledgements We thank Dagmar Gross and Nura Borger for technical assistance. We thank the Advanced Light Microscopy Facility (ALMF) at the European Molecular Biology Laboratory (EMBL) for support. We thank DFG for funding to SK. SK and GH were supported by AFI. SE was supported by funding of the TU (Technical University of Kaiserslautern) Nachwuchsring. We thank Daniel Romero Mujalli for his valuable support on the statistical analyses. We thank Dr. Sheue-Houy Tyan for encouragement to perform this study.

Compliance with ethical standards

Conflict of interest The authors declare no competing financial interests.

References

1. Hardy J, Selkoe DJ (2002) The amyloid hypothesis of Alzheimer's disease: progress and problems on the road to therapeutics. Science 297(5580):353–356
2. Kuhn PH et al (2010) ADAM10 is the physiologically relevant, constitutive alpha-secretase of the amyloid precursor protein in primary neurons. EMBO J 29(17):3020–3032
3. Vassar R et al (1999) Beta-secretase cleavage of Alzheimer's amyloid precursor protein by the transmembrane aspartic protease BACE. Science 286(5440):735–741
4. Lichtenthaler SF (2006) Ectodomain shedding of the amyloid precursor protein: cellular control mechanisms and novel modifiers. Neurodegener Dis 3(4–5):262–269
5. Lichtenthaler SF, Haass C, Steiner H (2011) Regulated intramembrane proteolysis—lessons from amyloid precursor protein processing. J Neurochem 117(5):779–796
6. Weidemann A et al (2002) A novel epsilon-cleavage within the transmembrane domain of the Alzheimer amyloid precursor protein demonstrates homology with Notch processing. Biochemistry 41(8):2825–2835
7. Sastre M et al (2001) Presenilin-dependent gamma-secretase processing of beta-amyloid precursor protein at a site corresponding to the S3 cleavage of Notch. EMBO Rep 2(9):835–841
8. Kang J et al (1987) The precursor of Alzheimer's disease amyloid A4 protein resembles a cell-surface receptor. Nature 325(6106):733–736
9. Brunholz S et al (2011) Axonal transport of APP and the spatial regulation of APP cleavage and function in neuronal cells. Exp Brain Res 217:353–364
10. Szodorai A et al (2009) APP anterograde transport requires Rab3A GTPase activity for assembly of the transport vesicle. J Neurosci 29(46):14534–14544
11. Boll W et al (2002) The mu2 subunit of the clathrin adaptor AP-2 binds to FDNPVY and YppO sorting signals at distinct sites. Traffic 3(8):590–600
12. Das U et al (2016) Visualizing APP and BACE-1 approximation in neurons yields insight into the amyloidogenic pathway. Nat Neurosci 19(1):55–64
13. Haass C et al (2012) Trafficking and proteolytic processing of APP. Cold Spring Harb Perspect Med 2(5):a006270
14. Willnow TE, Andersen OM (2013) Sorting receptor SORLA—a trafficking path to avoid Alzheimer disease. J Cell Sci 126(Pt 13):2751–2760
15. Haass C et al (1992) Targeting of cell-surface beta-amyloid precursor protein to lysosomes: alternative processing into amyloid-bearing fragments. Nature 357(6378):500–503
16. Lammich S et al (1999) Constitutive and regulated alpha-secretase cleavage of Alzheimer's amyloid precursor protein by a disintegrin metalloprotease. Proc Natl Acad Sci USA 96(7):3922–3927
17. Skovronsky DM et al (2000) Protein kinase C-dependent alpha-secretase competes with beta-secretase for cleavage of amyloid-beta precursor protein in the trans-golgi network. J Biol Chem 275(4):2568–2575
18. Kinoshita A et al (2003) Demonstration by FRET of BACE interaction with the amyloid precursor protein at the cell surface and in early endosomes. J Cell Sci 116(Pt 16):3339–3346
19. Fukumori A et al (2006) Presenilin-dependent gamma-secretase on plasma membrane and endosomes is functionally distinct. Biochemistry 45(15):4907–4914
20. Kaether C et al (2006) Amyloid precursor protein and Notch intracellular domains are generated after transport of their precursors to the cell surface. Traffic 7(4):408–415
21. Pasternak SH, Callahan JW, Mahuran DJ (2004) The role of the endosomal/lysosomal system in amyloid-beta production and the pathophysiology of Alzheimer's disease: reexamining the spatial paradox from a lysosomal perspective. J Alzheimer's Dis 6(1):53–65
22. Soba P et al (2005) Homo- and heterodimerization of APP family members promotes intercellular adhesion. EMBO J 24(20):3624–3634
23. Kaden D et al (2009) Subcellular localization and dimerization of APLP1 are strikingly different from APP and APLP2. J Cell Sci 122(Pt 3):368–377
24. Eggert S et al (2009) Induced dimerization of the amyloid precursor protein leads to decreased amyloid-beta protein production. J Biol Chem 284(42):28943–28952
25. Scheuermann S et al (2001) Homodimerization of amyloid precursor protein and its implication in the amyloidogenic pathway of Alzheimer's disease. J Biol Chem 276(36):33923–33929
26. Jung JI et al (2014) Independent relationship between amyloid precursor protein (APP) dimerization and gamma-secretase processivity. PLoS One 9(10):e111553
27. Isbert S et al (2012) APP dimer formation is initiated in the endoplasmic reticulum and differs between APP isoforms. Cell Mol Life Sci 69:1353–1375
28. Ben Khalifa N et al (2012) Structural features of the KPI domain control APP dimerization, trafficking, and processing. FASEB J 26(2):855–867
29. Hermey G et al (2006) Tumour necrosis factor alpha-converting enzyme mediates ectodomain shedding of Vps10p-domain receptor family members. Biochem J 395(2):285–293
30. Schmidt V et al (2007) SorLA/LR11 regulates processing of amyloid precursor protein via interaction with adaptors GGA and PACS-1. J Biol Chem 282(45):32956–32964

31. Hermey G et al (2015) SorCS1 variants and amyloid precursor protein (APP) are co-transported in neurons but only SorCS1c modulates anterograde APP transport. J Neurochem 135(1):60–75
32. Rabiej VK et al (2016) Low density lipoprotein receptor-related protein 1 mediated endocytosis of beta1-integrin influences cell adhesion and cell migration. Exp Cell Res 340(1):102–115
33. Altan-Bonnet N et al (2006) Golgi inheritance in mammalian cells is mediated through endoplasmic reticulum export activities. Mol Biol Cell 17(2):990–1005
34. Schilling S et al (2017) APLP1 is a synaptic cell adhesion molecule, supporting maintenance of dendritic spines and basal synaptic transmission. J Neurosci 37:5345–5365
35. Tyan SH et al (2012) Amyloid precursor protein (APP) regulates synaptic structure and function. Mol Cell Neurosci 51(1–2):43–52
36. Levites Y et al (2006) Anti-Abeta42- and anti-Abeta40-specific mAbs attenuate amyloid deposition in an Alzheimer disease mouse model. J Clin Investig 116(1):193–201
37. Nielsen MS et al (1999) Sortilin/neurotensin receptor-3 binds and mediates degradation of lipoprotein lipase. J Biol Chem 274(13):8832–8836
38. Del Turco D et al (2016) Region-specific differences in amyloid precursor protein expression in the mouse hippocampus. Front Mol Neurosci 9:134
39. Carpenter AE et al (2006) Cell Profiler: image analysis software for identifying and quantifying cell phenotypes. Genome Biol 7(10):R100
40. Baumkotter F et al (2014) Amyloid precursor protein dimerization and synaptogenic function depend on copper binding to the growth factor-like domain. J Neurosci 34(33):11159–11172
41. Clackson T (2006) Dissecting the functions of proteins and pathways using chemically induced dimerization. Chem Biol Drug Des 67(6):440–442
42. Munter LM et al (2007) GxxxG motifs within the amyloid precursor protein transmembrane sequence are critical for the etiology of Abeta42. EMBO J 26(6):1702–1712
43. Koo EH et al (1996) Trafficking of cell-surface amyloid beta-protein precursor. I. Secretion, endocytosis and recycling as detected by labeled monoclonal antibody. J Cell Sci 109(Pt 5):991–998
44. Andersen OM et al (2006) Molecular dissection of the interaction between amyloid precursor protein and its neuronal trafficking receptor SorLA/LR11. Biochemistry 45(8):2618–2628
45. Schmidt V et al (2012) Quantitative modelling of amyloidogenic processing and its influence by SORLA in Alzheimer's disease. EMBO J 31(1):187–200
46. Hermey G (2009) The Vps10p-domain receptor family. Cell Mol Life Sci 66(16):2677–2689
47. Yang M et al (2013) The intracellular domain of sortilin interacts with amyloid precursor protein and regulates its lysosomal and lipid raft trafficking. PLoS One 8(5):e63049
48. Gustafsen C et al (2013) Sortilin and SorLA display distinct roles in processing and trafficking of amyloid precursor protein. J Neurosci 33(1):64–71
49. Pietrzik CU et al (2004) FE65 constitutes the functional link between the low-density lipoprotein receptor-related protein and the amyloid precursor protein. J Neurosci 24(17):4259–4265
50. Wagner T, Pietrzik CU (2012) The role of lipoprotein receptors on the physiological function of APP. Exp Brain Res 217(3–4):377–387
51. Decock M et al (2015) Analysis by a highly sensitive split luciferase assay of the regions involved in APP dimerization and its impact on processing. FEBS Open Biol 5:763–773
52. Caporaso GL et al (1994) Morphologic and biochemical analysis of the intracellular trafficking of the Alzheimer beta/A4 amyloid precursor protein. J Neurosci 14(5 Pt 2):3122–3138
53. Palacios G et al (1992) Beta-amyloid precursor protein localization in the Golgi apparatus in neurons and oligodendrocytes. An immunocytochemical structural and ultrastructural study in normal and axotomized neurons. Brain Res Mol Brain Res 15(3–4):195–206
54. Guo Q et al (2012) Amyloid precursor protein revisited: neuron-specific expression and highly stable nature of soluble derivatives. J Biol Chem 287(4):2437–2445
55. Noda Y et al (2013) Copper enhances APP dimerization and promotes Abeta production. Neurosci Lett 547:10–15
56. Acevedo KM et al (2011) Copper promotes the trafficking of the amyloid precursor protein. J Biol Chem 286(10):8252–8262
57. Wang Q, Villeneuve G, Wang Z (2005) Control of epidermal growth factor receptor endocytosis by receptor dimerization, rather than receptor kinase activation. EMBO Rep 6(10):942–948
58. Schlessinger J (2002) Ligand-induced, receptor-mediated dimerization and activation of EGF receptor. Cell 110(6):669–672
59. Oved S, Yarden Y (2002) Signal transduction: molecular ticket to enter cells. Nature 416(6877):133–136
60. Nielsen MS et al (2001) The sortilin cytoplasmic tail conveys Golgi-endosome transport and binds the VHS domain of the GGA2 sorting protein. EMBO J 20(9):2180–2190
61. Waldron E et al (2008) LRP1 modulates APP trafficking along early compartments of the secretory pathway. Neurobiol Dis 31(2):188–197
62. Saito Y et al (2011) Intracellular trafficking of the amyloid beta-protein precursor (APP) regulated by novel function of X11-like. PLoS One 6(7):e22108
63. Guenette SY et al (1999) hFE65L influences amyloid precursor protein maturation and secretion. J Neurochem 73(3):985–993
64. Araki Y et al (2007) The novel cargo Alcadein induces vesicle association of kinesin-1 motor components and activates axonal transport. EMBO J 26(6):1475–1486
65. Konecna A et al (2006) Calsyntenin-1 docks vesicular cargo to kinesin-1. Mol Biol Cell 17(8):3651–3663
66. Ludwig A et al (2009) Calsyntenins mediate TGN exit of APP in a kinesin-1-dependent manner. Traffic 10(5):572–589
67. Aydin D, Weyer SW, Muller UC (2012) Functions of the APP gene family in the nervous system: insights from mouse models. Exp Brain Res 217(3–4):423–434
68. Kaden D et al (2012) The amyloid precursor protein and its homologues: structural and functional aspects of native and pathogenic oligomerization. Eur J Cell Biol 91(4):234–239
69. Khalifa NB et al (2010) What is the role of amyloid precursor protein dimerization? Cell Adhes Migr 4(2):268–272
70. Vooijs M et al (2004) Ectodomain shedding and intramembrane cleavage of mammalian Notch proteins is not regulated through oligomerization. J Biol Chem 279(49):50864–50873
71. Struhl G, Adachi A (2000) Requirements for presenilin-dependent cleavage of notch and other transmembrane proteins. Mol Cell 6(3):625–636
72. Kienlen-Campard P et al (2008) Amyloidogenic processing but not amyloid precursor protein (APP) intracellular C-terminal domain production requires a precisely oriented APP dimer assembled by transmembrane GXXXG motifs. J Biol Chem 283(12):7733–7744
73. Westmeyer GG et al (2004) Dimerization of beta-site beta-amyloid precursor protein-cleaving enzyme. J Biol Chem 279(51):53205–53212
74. Schmechel A et al (2004) Human BACE forms dimers and colocalizes with APP. J Biol Chem 279(38):39710–39717
75. Meckler X, Checler F (2016) Presenilin 1 and presenilin 2 target gamma-secretase complexes to distinct cellular compartments. J Biol Chem 291(24):12821–12837
76. Sannerud R et al (2016) Restricted location of PSEN2/gamma-secretase determines substrate specificity and generates an intracellular Abeta pool. Cell 166(1):193–208